

# WAVETRISK adaptive dynamical core coupled to dry physics

G Ching-Johnson<sup>1</sup>, NK-R Kevlahan<sup>2</sup>, T Dubos<sup>3</sup>, and F Hourdin<sup>4</sup>

<sup>1</sup>Department of Meteorology, University of Reading, Reading RG6 7BE, United Kingdom

<sup>2</sup>Department of Mathematics and Statistics, McMaster University, Hamilton ON L8S 4K1, Canada

<sup>3</sup>Laboratoire de Météorologie Dynamique, École Polytechnique, 91128 Palaiseau, France

<sup>4</sup>Laboratoire de Météorologie Dynamique, Institut Pierre Simon Laplace, Paris, France

**Correspondence:** Gabrielle Ching-Johnson (g.n.ching-johnson@pgr.reading.ac.uk)

**Abstract.** General circulation models (GCMs) of the atmosphere couple a dynamical core for fluid dynamics that are primarily two-dimensional with a physics model for processes like radiation and convection that are primarily one-dimensional. In this paper we fully describe the dry physics model of Hourdin (1992), which includes a soil column, radiation, vertical diffusion and convective adjustment. The climatology of the dry physics coupled with the WAVETRISK-ATMOSPHERE dynamical core is described. We show that the dynamically adaptive version of WAVETRISK-ATMOSPHERE can be stably and accurately coupled to the dry physics without scale-aware parameterizations or modifications to the dynamics-based adaptivity criteria. The turbulence generated by WAVETRISK–dry physics GCM is characterized by longitude-latitude projections of vorticity, three-dimensional vorticity isosurfaces and vertical profiles of energy spectrum power laws, which vary between  $-2.8$  in the boundary layer to  $-5.2$  in the stratosphere for the rotational mode.

## 10 1 Introduction

The coupling of atmospheric and oceanic General Circulation Models (GCMs) constitutes the backbone of global climate models (for which the acronym GCM is also used). Pioneered in the 1950's (Phillips, 1956), GCMs are specific numerical tools based on separating and coupling two fundamental components:

- 15 1. A “dynamical core” that computes the “large scale” fluid motions using approximate versions of the compressible or incompressible Navier–Stokes equations and transport of a thermodynamic prognostic variable, such as potential temperature or buoyancy.
  2. A set of “physics” models, called “parameterizations”, that account for physics other than fluid dynamics (e.g., radiation, phase changes, subsurface thermal conduction and hydrology). The physics includes subgrid scale (SGS) models to approximate the effect of unresolved fluid motions on the resolved scales (e.g., turbulent diffusion).
- 20 The parameterization of subgrid scale motions relies on Reynolds decomposition, which separates scales into a “large scale”, or average, resolved component on one side, and an unresolved turbulent component, or perturbation on the other. In the Reynolds decomposition framework, the large scale is defined formally as the ensemble average of random realizations of the full turbulent flow. In this decomposition, the statistics of the SGS variables are assumed to be horizontally homogeneous and

ergodicity is invoked to assume that ensemble averages are equivalent to both horizontal space and time averages (either a  
25 running mean, defined in each point of the continuous world, or a grid box average).

Similarly, the plane-parallel approximation is used for radiation. The radiation model assumes that all quantities are locally  
uniform horizontally, above a plane surface. For both SGS motions and radiation, the assumption of horizontal homogeneity  
results in physics models which are one-dimensional in the vertical.

GCMs, based on the separation of three-dimensional (fluid) dynamics and one-dimensional physics parameterizations, have  
30 proved to be very useful for understanding the climate machine, and in particular the link between convective and cloud  
processes and climate. From the beginning they have also been used successfully for prediction.

An early success, in the 1960s, was weather prediction over a time horizon of a few days. In the late 1970s climate models  
based on coupled atmospheric and oceanic GCMs successfully predicted the subsequent global warming. They played a great  
role in the raising concern about the risks of global warming. Today climate models are used systematically to model the climate  
35 at seasonal, decadal and centennial time scales. They are also used to evaluate the sensitivity of the climate to variations in  
input data, most importantly the level of greenhouse gas emissions. Although GCMs have reached a high degree of maturity  
and sophistication, many challenges remain.

Lastly, a major bottleneck of climate models is the enormous computational power and associated computational time  
required to produce useful results. Any increase in complexity, through the inclusion of more processes and higher resolution,  
40 requires more computational power. With only limited computational power, modellers are required to make numerous trade-  
offs between CPU time, physical and numerical accuracy, and the number of physical processes represented.

Choosing horizontal grid resolution  $\Delta x$  is the fundamental trade-off when designing and running a climate model. More  
resolution provides higher accuracy, but greatly increases the computational cost. Since the time step  $\Delta t \propto 1/\Delta x$ , doubling the  
resolution from  $\Delta x$  to  $\Delta x/2$  means a simulation year takes 8 times longer to compute on a given CPU (assuming memory is  
45 not a limitation), and in any case 8 times more operations must be done. This is the main motivation for dynamically adaptive  
grids, in which the resolution is refined locally depending on the time-dependent structure of the flow. Note that in practice  
only the horizontal resolution is adapted, even if Lagrangian vertical coordinates with adaptive remapping and dormant layers  
could in principle provide vertical resolution adaptivity. Often, high resolution is not required everywhere and so uniformly  
increasing resolution wastes computational resources: some regions are over-resolved at some times and others remain under-  
50 resolved. Dynamically adaptive climate simulations have been proposed as a way of using computational resources optimally  
and ensuring uniform accuracy (e.g., Jablonowski et al., 2004; Kevlahan and Dubos, 2019a). A dynamically adaptive GCM  
locally refines and coarsens the grid as a function of time and location based on dynamical, physical or numerical accuracy  
criteria (Jablonowski et al., 2004). Beyond capturing the evolution of the small scale dynamics, adaptivity aids in capturing the  
effects of the interactions between small-scale and large scale processes (Jablonowski et al., 2004).

55 In theory, adaptive grids could improve the realism and accuracy of model simulations, but there are known complications  
and challenges that come with adaptivity. Most notably, as mentioned above, SGS physics parameterizations are often designed  
for a particular horizontal resolution and may not perform properly when the grid is refined and coarsened during the simula-  
tion (Collins et al., 2013). This is expected to be the case for moist deep convection, when the grid resolution reaches a few

tens of kilometres, or for dry or cloudy boundary layer convection for resolutions of 1 or 2 km (Honnert, 2016). The question  
60 of whether physics processes should be “scale-aware” in this “grey zones” of convection is a challenge that many researchers  
are actively exploring (e.g., Frassoni et al., 2018; Park et al., 2022).

Scale-aware physics parameterizations adjust themselves based on the current local resolution of the grid. At its most basic,  
a scale-aware physics parameterization adjusts its internal model appropriately in response to changes in local grid resolution.  
A simple example is resolution dependent grid-scale viscosity, where the non-dimensional viscosity  $\nu\Delta t/\Delta x^2$  is kept constant  
65 when the grid resolution  $\Delta x$  changes. In the most extreme case where the resolution is refined enough to allow for the process  
to be fully resolved, the SGS parameterization is deactivated. Specifically, in the case of dynamic adaptivity, a refinement  
criteria needs to be met before local refinement (or coarsening) can occur. A central challenge of adaptivity is whether these  
criteria needs to be based on both the physics and the dynamics, or where adapting on the dynamics alone is sufficient. The  
answer likely depends on the type of physics being modeled. In current models the criteria are dynamics-based. For example,  
70 based on gradients or vorticity (e.g., St-Cyr et al., 2008), or based on the numerical approximation (e.g., Skamarock et al.,  
1989; Ferguson et al., 2016; Kevlahan and Dubos, 2019a). In order to make progress addressing these questions, researchers  
need well-understood physics models that can work in both the adaptive and non-adaptive models.

One strategy to tackle a particular bottleneck and test new approaches such as adaptive grids, is indeed to simplify other  
components or aspects of the model in order to avoid the complexity of running and analyzing results of a full GCMs. For  
75 example, models may be simplified by reducing the number or complexity of the components included. Atmospheric Global  
Climate Models (AGCMs) simulates the general circulation of the atmosphere, while an Atmospheric Ocean Global Climate  
Model (AOGCM) couples the ocean and atmosphere sub-models to simulate the general circulation. The atmosphere and ocean  
GCMs can also be more or less complex, and include more or fewer physical processes. When addressing bottlenecks that  
concern the atmospheric dynamics, the “physics” can be simplified further. The most basic atmosphere GCMs are hydrostatic  
80 and neglect topography, moist physics and ocean–atmosphere coupling. The land surface model is reduced to a basic radiation  
boundary condition and turbulent boundary layer model. Such highly simplified models are used to better understand physics–  
dynamics coupling and the effect of resolution. A classical way to develop new dynamical cores, or models, is to replace the  
atmospheric physics by a relaxation toward a prescribed latitude-altitude temperature field and include Rayleigh friction drag  
in the lowest layers to replace turbulent energy dissipation in the planetary boundary layer (Held and Suarez, 1994).

85 In this paper, we use a simple and versatile dry physics model developed by Hourdin (1992) to explore various atmospheric  
general circulation regimes for various planetary conditions. This model includes sub-models for radiation, convection, tur-  
bulence, the atmospheric boundary layer and the soil. This simple physics (with a few parameters modified) was used to  
investigate some aspects of the terrestrial atmospheric circulation. These included Hadley circulation and its sensitivity to  
planetary rotation rate and radiative properties, as well as the atmospheric circulation of Mars, Venus and Titan. It was also  
90 used to investigate atmospheric “superrotation” (?), a phenomenon dominates the circulation of Venus and Titan.

We chose this particular dry physics model to explore physics–dynamics coupling in a fairly realistic, yet simple, dry physics  
model with all assumptions and approximations fully described. The lack of moisture keeps the physics simple, but is still  
complex enough for us to investigate basic physics-dynamics coupling questions. By using dry physics, without phase change,

the scale at which parameterizations of SGS motions start to be questionable is reduced to a few kilometres. A strength of this physics model is that it can be easily coupled with different dynamical cores and adapted to model different planets, including gas giants. The final reason for focusing on this particular model is to fully document, implement and test a package that can be coupled to both adaptive and non-adaptive dynamical cores. This SGS physics parameterization package allows investigation of dynamic adaptivity, scale-awareness and the scale-dependence of basic physics processes, and could help reduce the need of climate model tuning with increases in resolution.

With these goals in mind, this paper presents the simple dry physics model in detail and evaluates its climatology in the non-adaptive and adaptive cases by coupling it to an existing dynamical core. This initial characterization of the simple physics model provides guidance on physics-dynamics coupling for adaptive GCMs, and introduces the simple physics package as a way of comparing different dynamical cores by coupling them to the same physics package. Specifically, this paper addresses the following key questions:

1. What is the climatology of the WAVETRISK–simple physics climate model? How does it differ from the Held and Suarez (1994) climate model?
2. Is the dynamically adaptive GCM numerically stable and able to capture the emergence of small scale structure? Is adaptivity efficient for seasonal climate simulations?
3. Is scale-aware dry physics and/or physics dependent adaptivity required for stable and accurate dynamically adaptive climate simulations?
4. Does the adaptive simulation capture the full range of active turbulent length scale in the atmosphere, as well as the correct power law scaling?
5. Can the WAVETRISK–simple physics climate model be restarted successfully from a checkpoint with significantly increased resolution?

The paper is organized as follows. Section 2 describes in detail the simplified dry physics model, explaining its components and discussing its assumptions, limiting features and potential improvements. Section 3 describes the coupling of the dry physics model with the adaptive dynamical core WAVETRISK (Kevlahan and Dubos, 2019b; Kevlahan and Lemarié, 2022) in both the adaptive and non-adaptive cases. Section 4 presents and interprets the results of the physics-dynamics coupling in the non-adaptive and adaptive cases, exploring the climatology and the effects of seasons, and Section 5 summarizes our conclusions and proposes future research directions.

## 2 Simple Dry Physics Model

This section introduces the simple dry physics model. We begin by summarizing the general model's assumptions ~~and then describe in detail each component of the model (before describing describe the various processes represented: radiation, turbulent diffusion, convection, planetary boundary layer, soil column), with a particular focus on.~~ These processes are treated

125 sequentially in a process splitting approach. A particular attention is given to the description of boundary conditions and time  
integration. ~~Lastly we~~ We describe the limitations of the package and its potential improvements. As with most physics models,  
the simple dry physics is is implemented as a time integration split step ~~and~~. It works on a set of vertical columns (of varying  
cross-section in the adaptive case). The fact that the dynamics works on individual horizontal layers (or quasi horizontal for  
non lagrangian vertical coordinate) and the physics works on individual vertical columns is a fundamental approximation of  
130 GCMs, ~~and~~. It is well-suited to horizontal grid adaptivity.

## 2.1 Physics model assumptions

~~To properly understand a physics model it is essential to explicitly state its assumptions and approximations. This not only  
allows for full~~ **Ce serait bien que Thomas reprenne cette sous-section**

Explicitelcaitation of the model physics assumption is essential not only for understanding and transparency, but also **avoids**  
135 to avoid inconsistent assumptions when the physics and dynamics are coupled (Lauritzen et al., 2022).

The basic assumptions of this physics package are: dry thermodynamics, compressible flow (i.e. atmosphere, not ocean),  
hydrostatic pressure, and a floating (Lagrangian) vertical hybrid coordinate.

**No moisture and compressibility approximations.** A fundamental approximation of this package is the assumption that  
moisture (e.g., water in its three phases) is not taken into account. In particular, condensible substances and their effects on the  
140 atmospheric dynamics are absent. Such models are called dry physics models. Secondly, the model assumes compressible flow,  
which means it is suitable for the atmosphere, not the ocean. A fluid is compressible if changes in pressure causes significant  
changes in density. When modeling the atmosphere, the density of dry air changes significantly with changes in atmospheric  
pressure. Therefore, these two basic assumptions of no moisture and compressibility need to be ensured when coupling with a  
dynamical core.

145 **Hydrostatic approximation.** Another fundamental approximation in this simple physics model is the hydrostatic vertical  
pressure. The coupled dynamical model must therefore also assume hydrostatic balance. The hydrostatic approximation con-  
strains the vertical coordinates in the model and simplifies the vertical equation of motion. An important implication of the  
hydrostatic approximation is that dry convection must be parameterized and cannot be resolved (even if the local grid resolution  
permits it).

150 **Floating vertical coordinate.** There are many possible spatial coordinate systems that can be used when modeling a planet.  
For example, the Cartesian coordinate system, with coordinates  $(x, y, z)$ , where  $z$  is the vertical height above mean sea level.  
In the case of simplified AGCMs, where the dynamics and the physics are coupled, the dynamics works on two-dimensional  
layers and the physics works on one-dimensional vertical columns. While  $z$  might be one's first choice for a vertical coordinate,  
other possible vertical coordinates include pressure, mass and sigma (a normalized pressure coordinate).

155 Vertical fluxes of heat causes air parcels to expand and compress, and in turn change the density  $\rho$  (and associated buoyancy),  
which is represented in the mass continuity equation by

$$\frac{\partial \rho}{\partial t} + \frac{\partial}{\partial z}(w\rho) = 0, \quad (1)$$

where  $w$  is the vertical velocity.

160 When altitude  $z$  is the vertical coordinate there are vertical fluxes across the horizontal layers and the dynamics must include vertical velocity as a prognostic variable (in addition to horizontal velocities in each layer). The vertical velocity must be diagnosed from the density, which can be a tedious process. An easier option, implemented in this physics package, is to use a Lagrangian vertical coordinate, sometimes known as a floating vertical coordinate, so there is no mass flux across horizontal layers. In the case of a Lagrangian vertical coordinate  $\zeta$ , the  $z$  coordinate has the form  $z = z(\zeta, t)$  and there is no explicit vertical velocity (and no mass flux across vertical layer interfaces) since the horizontal layers move vertically with the local vertical velocity. Therefore, the incremental mass  $dM$  is

$$dM = \rho dz = m d\zeta = \rho \frac{\partial z}{\partial \zeta} \partial \zeta \quad (2)$$

and  $dM/dt = 0$ , where  $m = \partial M/\partial \zeta = \rho \partial z/\partial \zeta$ . Note that since the thickness of the horizontal layers changes over time, the vertical coordinates must be remapped periodically onto the initial vertical coordinates, or optimized target vertical coordinates.

## 2.2 Model parameterizations

170 The physics package includes parameterizations for radiation, vertical turbulent diffusion of velocity and potential temperature, a planetary boundary layer surface scheme, dry convective adjustment, soil column (for realistic surface flux boundary conditions), and diurnal radiation forcing. All models are one-dimensional (vertical) in space, and therefore are applied independently to each one-dimensional vertical column on the sphere as an implicit split step after the dynamics time step (i.e., the physics package takes as input a set of vectors). Note that none of the physics sub-models explicitly require the horizontal cross-section of the column (i.e., its horizontal resolution), although horizontal grid resolution could implicitly modify the physics models and physics–dynamics coupling. This is one of the questions we are interested in.

The time scheme for the physics step uses Strang splitting:

1. Explicit forward Euler for soil, surface flux, radiation, and dry convective adjustment.
2. Implicit backwards Euler for vertical turbulent diffusion of velocity and potential temperature.

180 In the following, we give full details of each sub-model, including their default parameters. More details on the physics time scheme is given in Section 2.5.1.

### 2.1.1 Radiation

~~Radiation is a process that has a major impact on the atmosphere. In general, since radiation is not a dynamical process and due to its complexity, its parameterization involves a hierarchy of simplifying assumptions (e. g.,~~

## 185 2.2 Radiation

Absorption of solar radiation by the atmosphere and surface is the first driver of the atmospheric circulation. Then the atmosphere and surface emits thermal radiation, essentially in the infra-red spectrum, which is then absorbed by the surface

190 and atmosphere, or emitted back to space. The modification of the efficiency of the atmosphere to emit and absorb thermal radiation is at the origin of the on going global warming. As is the case for the dynamical core based on a simplified version of the well established Navier-Stokes equations, radiative codes in GCMs rely on the well established transfer equation for local thermodynamic equilibrium, ~~only vertical radiative transfer, simplified or neglected scattering, discretized spectral bands, ...~~. The integration of this equation in all its spacial and spectral dimensions is however far from practicable in GCMs, and this by orders of magnitudes of computer time. Many classical approximations are thus used in operational codes, which are even simplified further here as detailed bellow.

195 ~~The radiation model included in the physics package is based on the two-stream approximation. The two-stream approximation equations make the plane-parallel assumption, in which radiation is a function of height and the atmosphere is horizontally homogeneous and stratified in flat, horizontal layers (at least on the horizontal scale of the column~~ **We could put the general radiative transfer equation here. But not sure it is useful.**

### 2.2.1 Approximations of the radiative transfer equation

200 The main approximations used when integrating radiative transfer in a climate or weather forecast model are the following:

The separation of solar radiation and terrestrial radiation is made possible and is not an approximation because the radiative transfer equation is linear with respect to its sources: here the solar emission for solar radiation and the thermal emission by the atmosphere and planetary surface for the "terrestrial" or "thermal" or "long-wave" radiation.

205 The plan parallel approximation is used in all the GCM codes. It consists in assuming that all the atmospheric properties depends on altitude only on an infinite horizontal plane. The approximation extends to the statistics of clouds (clouds may vary horizontally but there distribution is the same everywhere in this plane). ~~The resulting downward and upward radiation fluxes at a specific frequency  $\nu$  and height  $z$  are-~~

$$\begin{aligned}
 \underline{F_+(\nu, z)} &= \underline{F_+(\nu, 0)\tau(\nu, 0, z) + \int_0^{z'} \pi B(\nu, T(z'))K(\nu, z')\tau(\nu, z', z) dz'} \\
 &= \underline{F_+(\nu, 0)\tau(\nu, 0, z) + \int_0^{z'} \pi B(\nu, T(z')) \frac{\partial \tau(\nu, z', z)}{\partial z'} dz'} \\
 \underline{F_-(\nu, z)} &= \underline{F_-(\nu, \infty)\tau(\nu, z, \infty) + \int_{z'}^{\infty} \pi B(\nu, T(z'))K(\nu, z')\tau(\nu, z, z') dz'} \\
 &= \underline{F_-(\nu, \infty)\tau(\nu, z, \infty) - \int_{z'}^{\infty} \pi B(\nu, T(z')) \frac{\partial \tau(\nu, z, z')}{\partial z'} dz'},
 \end{aligned}$$

210

where the + subscript indicates an upward flux and the — subscript indicates a downward flux.  $B(\nu, T(z'))$  is Planck's function:-

$$\underline{B(\nu, T(z')) = \frac{2h\nu^3}{c^2(e^{h\nu/kT(z')} - 1)},}$$

215

where  $h$  is Planck's constant. Planck's function describes the radiation emitted by a black body in thermal equilibrium at a given temperature  $T(z')$ .

$\tau_\nu(z, z')$  is the transmission function, which represents the proportion of the incident radiation, at frequency  $\nu$ , which is emitted from layer  $z$  to layer  $z'$ . Therefore, it is the proportion of the flux that is not absorbed and in this model it is crudely represented by-

$$\tau(z, z') = e^{-|\psi(z) - \psi(z')|^\alpha},$$

plan parallel approximation results in radiative transfer models which are purely 1D on the vertical. where  $\psi$  is a monotonic function and  $\alpha$  represents the absorption weight. This is known as a band-averaged transmission function, as it approximates the transmission function over a given frequency band. The particular transmission function differs depending on the radiation band, thus the monotonic function in the physics package depends on the frequency band-

**The two stream approximation** consists in replacing the integral on angles by only two directions, one upward and one downward. It can be seen as a particular case of the discrete ordinate method, which consists in integrating on a discrete number of angles. Here the integration is restricted to two angles. The model computes separately downward and upward fluxes, assuming that the attenuation is done as if all the photons were transported along a unique direction. The solar beam is of course integrated along the real solar zenith angle  $\Theta_S$ , considering all photons which have not been scattered at the surface or in the atmosphere (correcting often the atmospheric scattering from its forward propagation with the Delta Eddington approximation). In this framework, the solar radiation is split between direct and indirect diffuse radiation. For both the thermal infrared radiation and for the diffuse solar radiation, and for both upward and downward fluxes, the zenith angle of propagation of light  $\Theta_0$  is chosen according to the **diffusive approximation**, with  $\mu_0 = 1/\cos\Theta_0 = 5/3$ . In general, transmission functions are multiplicative. However, due to band-averaging of the transmission function this property is lost.

$K(\nu, z')$  represents the absorption, at layer  $z'$ , of radiation at frequency  $\nu$ , and is dependent on the infrared absorbers (i.e. gas) in the atmosphere,

$$K(\nu, z') = \sum_i \rho_i \kappa_i(p, T, \nu),$$

where  $\kappa(p, T, \nu)$  is the absorption coefficient of gas  $i$

**Approximations for the spectral integration** are of various nature. For the atmospheric gas, coefficients for absorption and scattering have a very complex spectral signature made of billions of absorption lines associated with quantum energy transition levels of three-atomic molecules. Line-by-line integrations consisting of taking into account all the individual transition lines is far from practicable in GCMs. Various possibilities of Band models are used in GCMs, summarizing the absorption over a finite spectral intervals. Those models consists either of learning functions based on line-by-line integration, or in k-distribution or k-correlated approaches in which the integration on frequencies within a given band is replaced by an integration over values of the absorption coefficient.

Further simplifications are used here. First scattering is neglected. Scattering couples all the direction in the radiative transfer equation. Even in the two stream approximation, it couples the equations of the direct solar radiation and  $\rho$  is the density of the gas  $i$ . The simple physics model assumes that the absorption coefficients depend only on height that of the tho diffuse angle associated with upward and downward solar radiation. It couples as well the downward and upward fluxes for the terrestrial radiation. Neglecting scattering simplifies a lot the computation. For the solar radiation in particular, the downward radiation is computed purely along the solar zenith angle while the upward radiation is only diffuse (as is always the case if not accounting for specular reflection by the surface). The second simplification concerns the spectral integration. The extinction is assumed independent of the frequency. In the pure "grey" approximation, i.e. with no variation of the gaz absorption coefficient, the transmission  $\tau$  along zenithal angl  $\Theta$  reads

The equations of the resulting radiative code are derived bellow.

~~The simple physics model assumes constant absorption coefficients for~~

### 2.2.2 Integration for the terrestrial or long-wave radiation

The net radiative flux in the longwave (visible)-or terrestrial or thermal) radiation reads is the sum of and upward ( $F_L^\uparrow$ ) and shortwave (visible) bands. The longwave (infrared) absorption coefficient is  $\kappa_L = 0.08$  and the shortwave (visible) absorption coefficient is  $\kappa_S = 0.99$  downward ( $F_L^\downarrow$ ) flux:  $F_L(z) = F_L^\uparrow(z) - F_L^\downarrow(z)$ .

In general, the transmission function  $\tau_\nu$  is a function of  $K(\nu, z')$ . Due to the band averaging of Let us first consider just the upward thermal radiation, averaged over the zenith angles in a half-space. Without scattering and in a two stream approach, the monochromatic equation of radiative transfer integrated on the above half-space reads

$$F_L^\uparrow(\nu, z) = F_L^\uparrow(\nu, 0)\tau_\nu(0, z) + \int_0^z \pi B_\nu[T(z')] K_\nu(z') \tau_\nu(\mu_0, z', z) \mu_0 \rho dz' \quad (3)$$

where  $B_\nu[T(z')]$  is Planck's function:

$$B_\nu[T(z')] = \frac{2h\nu^3}{c^2(e^{h\nu/kT(z')} - 1)}, \quad (4)$$

where  $h$  is Planck's constant. Planck's function describes the radiation emitted by a black body in thermal equilibrium at a given temperature  $T(z')$ .  $K_\nu(z)$  is the absorption coefficient per unit mass of air and

$$\tau_\nu(\mu_0, z, z') = \exp \left[ - \int_z^{z'} K_\nu(z'') \mu_0 \rho dz'' \right] \quad (5)$$

is the transmission function,  $K(\nu, z')$  is not explicitly defined. However the band-averaged transmission function does describe strong or weak absorption of a frequency band through  $\alpha$ . A strong absorption produces a steep decay of transmission and strong absorption of radiation over shorter paths (Pierrehumbert, 2010). This means that for longer paths the absorption in the

275 first part of the path is stronger, while a absorption is weaker further along in the path. Therefore, strong absorption is usually used for frequencies that are absorbed first in a path.

To solve for the net upward transmission function, i.e. the fraction of incident radiation, at altitude  $z$  and frequency  $\nu$ , which is received at altitude  $z'$ . Eq. 3 expresses the upward flux at altitude  $z$  as the sum of the surface emission after attenuation between the surface and altitude  $z$ , and of the sum of the emissions (after attenuation between  $z'$  and downward irradiance, the fluxes need to be integrated over all frequencies. The physics packages uses the dual band two-stream approximations by crudely integrating the fluxes over just two spectral bands, longwave (L) and shortwave (S). Therefore, the net flux of radiation is  $z$ ) from all the altitudes  $z'$  below  $(\pi B_\nu [T(z')] \mu_0 \rho dz')$  for a layer of thickness  $dz'$ . The coefficient  $\mu_0$  accounts for the fact that the atmospheric optical depth used in emission (Eq 3) and absorption (Eq 5) is computed along the mean zenith angle  $\Theta_0$ .

285 Noticing that the derivative of the transmission function appears in the integral, and assuming that the surface emits as a black body (emissivity equal to unity), this equation can be rewritten as:

$$F_+(\nu, z) = \pi B_\nu [T_s] \tau_\nu(0, z) + \int_0^{z'} \pi B_\nu [T(z')] \frac{\partial \tau_\nu(z', z)}{\partial z'} dz' \quad (6)$$

If the transmission function is independant of  $\nu$ , the equation can be integrated on the full spectrum and reads:

$$F_{rad} = \int_0^\infty F_-(\nu, z) - F_{++}(\nu, z) d\nu = F_L \sigma T_s^4 \tau(0, z) + F_S \int_0^{z'} \sigma T^4(z') \frac{\partial \tau(z', z)}{\partial z'} dz' \quad (7)$$

290 where  $F_L$  and  $F_S$  are respectively the net longwave and shortwave radiation fluxes using the Stefan-Boltzmann law (Pierrehumbert, 2010) where  $\sigma = 5.67 \times 10^{-8} \text{ W m}^{-2} \text{ K}^{-4}$  is the Stefan-Boltzmann constant.

This equation is integrated here with a straightforward finite differences, conservative scheme, as

$$F_L^\uparrow(l + \frac{1}{2}) = \sigma T_s^4 \tau(0, l + \frac{1}{2}) + \sum_{k \leq l} \left[ \tau(k + \frac{1}{2}, l + \frac{1}{2}) - \tau(k - \frac{1}{2}, l + \frac{1}{2}) \right] \sigma T(k)^4, \quad (8)$$

A very similar form is used for the downward flux:

$$F_L^\downarrow(l + \frac{1}{2}) = \sum_{k > l} \left[ \tau_L(l, k - \frac{1}{2}) - \tau_L(l, k + \frac{1}{2}) \right] \sigma T(k)^4 \quad (9)$$

295 J'ai pris les notations avec des 1/2 pour coller avec ce qui est fait plus loin sur la couche limite, mais on peut changer ça

### 2.2.3 Shortwave Integration for the solar radiation

The shortwave net flux is the net result of the upward and downward fluxes evaluated for shortwave radiation,

$$F_S(z) = F_{S+}(z) - F_{S-}(z). \quad (10)$$

300 ~~The simple physics case neglects atmospheric emission of shortwave radiation, leaving the single initial terms as the upward and downward flux. Since the unique source accounted for in this part of the code is the emission by sun, and because scattering is neglected, the integration for the solar radiation, reads (after integration over the full spectrum):~~

$$F_{S-}(z) = \tau_S(z, \infty) \mu S \quad (11)$$

$$F_{S+}(z) = \tau_S(0, z) F_{S+}(0) \quad (12)$$

where  $S$  is the downward flux at the top of the atmosphere, which in the case of shortwave radiation is the solar flux and  $\mu$  is the cosine of the zenith angle. ~~The solar flux represents the amount of flux from the solar star impinging on the outer atmosphere. The upward flux at height  $z$  (Equation 12) represents the proportion of the upward flux at the ground transmitted through the atmosphere, while the downward flux represents the proportion of the incident solar flux transmitted through the layer at  $z$ . Look in the code, but the angle should not be the same for the direct downward radiation and diffuse upward radiation~~

310 The boundary upward flux of radiation,  $F_{S+}(0)$ , is the portion of downward shortwave radiation that is reflected by the ground,

$$F_{S+}(0) = -(1 - \alpha) F_{S-}(0), \quad (13)$$

where  $\alpha$  is the albedo, which depends on the reflective properties of the ground ( ~~$\alpha \approx 1$  for fresh snow,  $\alpha \ll 1$  for  $\alpha \approx 0.1$  for oceans or forests~~). The albedo  $\alpha = 0.112$  for our simulations, independent of position, although the physics package allows location-dependent albedo (e.g., different for land and ocean regions). ~~Therefore there is no shortwave radiation emitted by the ground itself, however the ground does emit longwave (heat) radiation and is taken into consideration in the longwave fluxes described below.~~

320 ~~The transmission factor  $\tau_S$  for the shortwave spectral band depends on height according to~~

$$\tau_S(z, \infty) = e^{-c_S \frac{\psi(z)}{\mu}},$$

$$\tau_S(0, z) = e^{-c_S \frac{\psi(0) - \psi(z)}{\mu_0}},$$

$$320 \quad \psi(z) = \frac{p(z)}{p_{rad}},$$

~~where  $p_{rad} = 1000$  is a reference pressure height and  $c_S = 0.005$  is the attenuation of shortwave radiation at pressure height  $p_{rad}$ .  $\mu$  is the cosine of the zenith angle and  $\mu_0$  is an average of  $\mu$ ,  $\mu_0 = 3/5$ .~~

## 2.2.4 Transmission function

## 2.2.5 Longwave radiation

325 ~~The longwave radiative fluxes in the simple physics package are represented using the gray gas approximation of the two-stream equations. As in the case of the shortwave net flux, In the most general case, the longwave net flux is determined by absorption coefficient  $K_\nu$  entering in the definition of the transmission function  $\tau_\nu$  (Eq. 5), depends upon the absorbers (i.e. gas) in the~~

atmosphere,  $K_\nu(z) = \sum_i \rho_i \kappa_i(p, T, \nu)$ , where  $\kappa_i(p, T, \nu)$  is the absorption coefficient of gas  $i$  and  $\rho_i$  is the density of gas  $i$ . Each coefficient  $\kappa_i$  is the sum of “lines” of absorption, each line being a function of  $p, T$  and  $\nu$ .

330 The most drastic approximation of this absorption spectrum is the so-called grey gas approximation which consists in assuming that we have a single gas with constant absorption  $K_{\nu 0}$ , in which case the transmission function simply reads:

$$F_L \tau(\mu, z) = F_{L+}(z') = \exp \left( -F_{L-}(\mu K_{\nu 0} \int_z^{z'} \rho dz) \right) \quad (14)$$

where  $F_{L+}(z)$  and  $F_{L-}(z)$  represent the upward and downward longwave fluxes respectively.

335 A further assumption in the gray gas model is the neglect of longwave solar emission meaning  $F_{L-}(\infty) = 0$ . Also, since the longwave radiative fluxes are the result of the two-stream approximations (??) integrated over infrared frequencies, the integration over infrared frequencies of the second term is well approximated by the Stefan-Boltzmann law (Pierrehumbert, 2010). More specifically,

$$\int \pi B \frac{\partial}{\partial z'} \tau(\nu, z, z') d\nu \approx \sigma T(z)^4 \frac{\partial}{\partial z'} \tau_L(z, z'),$$

340 where  $\sigma = 5.67 \times 10^{-8} \text{ W m}^{-2} \text{ K}^{-4}$  is the Stefan-Boltzmann constant. Therefore, the downward and upward flux of longwave radiation can be approximated as

$$F_{L-}(z) = \int F_- d\nu = - \int \sigma T(z')^4 \frac{\partial \tau_L(z, z')}{\partial z'} dz'$$

$$F_{L+}(z) = F_{L+}(z=0) \tau_L(0, z) + \int \sigma T(z')^4 \frac{\partial \tau_L(z', z)}{\partial z'} dz'.$$

or

$$\tau(\mu, z, z') = \exp \left( - \frac{\mu K_{\nu 0}}{g} |p(p) - p(z')| \right) \quad (15)$$

345 The transmission factor  $\tau_L$  for the shortwave spectral band depends on height according to (14), but with strong absorption coefficient  $C_L = 2.53$ . transmission between pressure level  $p$  and  $p'$ , assuming that the atmosphere is in hydrostatic balance. With this approximation, the transmissivity remains multiplicative ( $\tau(\mu, z_0, z_1) = \tau(\mu, z_0, z_1) \tau(\mu, z_1, z_2)$ ), a fundamental property of monochromatic radiative transfer.

350 The upward surface boundary radiation flux is comprised of the heat flux emitted from the ground itself and the fraction of the downward atmospheric longwave radiation that is reflected by the ground (i.e., not absorbed by the ground). Therefore, This form of the transmission function is valid when the atmosphere is optically thin. It produces however vertical profiles that are much more stable than those generally observed in the tropospheres of terrestrial planets, where the upper layers of the atmosphere are directly heated by surface radiation. In the tropospheres of terrestrial planets, the significant molecular bands are generally saturated very quickly, and exchanges between distant layers are possible only within certain windows that generally play a minor role in the radiative budget.

355

When integrating radiation for a single absorption line, two extreme approximations can be considered: a thin layer approximation where  $\ln\tau$  is linear with respect to the mass of absorber encountered and scales with  $\Delta p$ , and a thick layer approximation, where the line is saturated in its center, so that the effective absorption increases as the width of the saturated band. In this case, the transmission function scales with  $\sqrt{\Delta p^2}$ . With this dependency, a larger fraction is absorbed at short distance. (Pierrehumbert, 2010).

Here the strong approximation is used for the thermal terrestrial radiation and the thin approximation is used for the solar radiation.

The transmission function for the solar radiation is finally computed assuming a thin approximation as

$$F_{L+}(0)\tau_S(\mu_S, z, z') = \epsilon\sigma T_s^4 + \exp\left(-c_S|\psi(1-\epsilon z)F_{L-}(0), -\psi(z')|\right) \quad (16)$$

where  $\epsilon = 1$  and  $T_s$  are the soil emissivity and the surface temperature. The emissivity and the albedo, mentioned in the shortwave section are both characteristics of the ground, but they describe the effects for different wavelengths. The albedo  $\alpha$  is the fraction of shortwave radiation reflected by a surface, while the emissivity is the effectiveness of a surface, the ground in this case, to emit longwave (heat) radiation. Both parameters are an input to the initialization of the physics package. Rearranging (??) gives the net longwave flux at the boundary,

$$F_L(0) = F_{L+}(0) - F_{L-}(0) = \epsilon(\sigma T_s^4 - F_{L-}(0)).$$

The transmission factors for the longwave spectral band are represented as

$$\tau_L(z, z') = e^{-c_{LW}\sqrt{|\psi(z') - \psi(z)|}}$$

$$\psi(z) = \left(\frac{p(z)}{p_{rad}}\right)^2,$$

where  $c_{LW} = 2.53$ ,  $\psi(z) = p(z)/p_{rad}$  and  $\mu_S$  is the solar zenith angle. The reference pressure,  $p_{rad} = 1000$  hPa, is introduced so that that the transmissivity of the atmosphere computed from the surface  $p \simeq p_{rad}$  to the top of the atmosphere ( $z = \infty$  and  $p = 0$ ) is  $\tau_S(\mu, 0, \infty) = \exp(-c_S)$ . We choose  $c_S = 0.005$  is the attenuation of the longwave-shortwave radiation at pressure height  $p_{rad} = 1000$ . (A weak absorption option is also available for longwave radiation with  $\psi(z) = p(z)/p_{rad}^2$ .)

Upon discretization, the longwave equations are computed as,

$$F_{L-}(l) = \sum_{k>l} (\tau_L(l, k_-) - \tau_L(l, k_+))\sigma T(k)^4$$

$$F_{L+}(l) = F_{L+}(z=0)\tau_L(0, z) + \sum_{k<l} (\tau_L(k_+, l) - \tau_L(k_-, l))\sigma T(k)^4,$$

Regarder cette histoire d'angle direct et diffus.

For the long-wave transmission, we use the strong absorption approximation

$$\tau(\mu, z, z') = \exp\left(-c_L\sqrt{|\psi(z') - \psi(z)|}\right) \quad (17)$$

$$\psi(z) = \left(\frac{p(z)}{p_{rad}}\right)^2, \quad (18)$$

Parameter	Value
Solar constant	1370 W m <sup>-2</sup>
Perihelion distance	150 × 10 <sup>6</sup> km
Ellipticity	0
Orbital period	1 year
Planet radius	6371 km
Gravitational acceleration $g$	9.8 m s <sup>-2</sup>
Reference temperature $T_0$	285 K
Obliquity	23.5°
Rotation $\Omega$	7.292 × 10 <sup>-5</sup> rad s <sup>-1</sup>
Day length	24 h

**Table 1.** Astronomical parameters used for the simple physics package (based on Earth values).

385 where  $l$  is the layer interface and  $k$  is the center of the layer. Therefore  $k_+$  and  $k_-$  represent the interfaces above and the below  
layer  $k$  respectively with  $C_L = 2.53 \text{ m}^{-1}$ , so that the transmission of the whole atmospheric columns is  $\tau(\mu 0, 0, \infty) = \exp(-C_L) = 0.08$ .

Vérifier les valeurs

### 2.2.5 Integration in the climate model

390 The warming or cooling of a layer is affected by the net change in radiation with height, and is derived from the conservation  
of energy equation. This gives an expression for the temperature tendency,

$$\frac{\partial T}{\partial t} = -\frac{1}{\rho c_p} \frac{\partial F_{rad}}{\partial z}, \quad (19)$$

where  $c_p = 1004 \text{ J kg}^{-1} \text{ K}^{-1}$  is the specific heat capacity of air (Arya, 1988) and  $F_{rad} = F_L(z) + F_S(z)$

Finally, the change in net radiative surface boundary flux with respect to the surface temperature is

$$\frac{\partial F_{rad}(l)}{\partial T_s} = 4\epsilon\sigma T_s^3 \tau_L(0, l). \quad (20)$$

395 This relation is used for the implicit coupling at the boundary.

### 2.2.6 ~~Astronomical parameters and diurnal cycle~~

The radiative transfer model is forced by solar radiation, which is time-dependent and set by the planet's astronomical parameters (e.g., obliquity, which determines seasons) and the diurnal (day/night) cycle. In this paper we set these parameters to their Earth values, which are listed in Table 1. The physics package includes a flag that activates diurnal radiation forcing.

## 400 2.2.6 Vertical turbulent diffusion

### 2.3 Subgrid scale motions

Turbulence has a major impact on the dynamics of atmospheric flow. In general, turbulence spans a large range of spatial and time scales, from sub-millimetre to kilometres. More importantly for us, the computational cost of computing an integral time scale of a homogeneous three-dimensional turbulent flow scales like  $Re^3$ , where  $Re$  is the non-dimensional Reynolds number characterizing the turbulence. Since  $Re = O(10^8)$  for the atmosphere, it is clear that turbulence cannot be fully represented at the resolved scales and at least some turbulent length scales must be parameterized. This parameterization represents the effects of turbulence at the unresolved small scales on the resolved large scales.

In GCMs turbulence, like other dynamics and physics, is decomposed into its horizontal and vertical components. In our simulations, and climate simulations in general, the inertial (power law energy spectrum) range of horizontal turbulence is partially resolved. Since the minimum resolution is in the inertial range the unresolved horizontal turbulence needs to be modeled. In our case, we use second-order hyperdiffusion (i.e.  $\nu_2 \Delta^2 u$ ) to model the effect of unresolved turbulence on the resolved turbulence as diffusion. The kinematic viscosity  $\nu_2$  is chosen to be the minimum required to remove grid-scale noise based on the non-dimensional viscosity. In the adaptive case, diffusion can either be based on the maximum grid resolution, or it can be scale-aware (based on the local grid resolution). It is also possible to use more sophisticated horizontal turbulence models, such as large eddy simulation (LES).

In contrast, GCMs never resolve any part of the the vertical turbulence in each column: the effect of vertical turbulence is modeled as an enhanced vertical diffusion of velocity and potential temperature. The goal of these models is therefore to approximate the vertical ~~turbulent viscosity transport by subgrid motions~~ for velocity and temperature (i.e., eddy viscosity, turbulent diffusivity) for each column based on inputs from the dynamics step.

#### 420 2.3.1 Turbulent diffusion

The simplest and most common model for vertical turbulent ~~viscosity transport is the so called eddy-diffusion or turbulent diffusion which acts as a viscosity.~~

A simple approach for turbulent diffusion is the first-order ~~one~~ equation mixing length closure approximation. ~~Ocean models State-of-the-art ocean~~ (such as NEMO~~use the~~) ~~or atmospheric (such as LMDZ) GCMs use~~ second-order ~~closure-closures like~~  $k$ - $\epsilon$  model, which solves a coupled dynamical system for vertical turbulent kinetic energy (TKE)  $k$  and turbulent dissipation  $\epsilon$  in order to compute the the effective turbulent viscosity coefficients.

Recall that the prognostic variables are assumed to be quantities averaged over large scales  $L$  and long times  $T$  (i.e. they are the “large scale” or coarse-grained resolved by the dynamics model). The effect of the unresolved vertical turbulence on the prognostic variables in each layer is modeled as an enhanced vertical diffusion in their tendencies. The vertical turbulent diffusion model therefore converts a portion of the horizontal TKE into heat at a rate  $\epsilon$  that depends on the diffusion coefficient  $K_z^u$  and the vertical shear  $\partial_z \mathbf{u}$ . To ensure conservation of energy,  $\epsilon$  must be included as a source term in the heat equation (27). Vertical turbulent diffusion also transfers velocity and potential temperature between horizontal layers.

Since turbulence is assumed to act as an enhanced diffusion, the vertical flux of a quantity  $q$  is given by

$$F_q = -\rho K_z^q \frac{\partial q}{\partial \zeta}, \quad (21)$$

435 where  $\rho$  is the density,  $K_z^q$  is a variable turbulent viscosity (to be modeled), and  $\partial q / \partial \zeta$  is the vertical gradient of  $q$ .

In general, the turbulent viscosity  $K_z^q$  depends on the variable  $q$ . However, the physics package assumes that this coefficient is the same for both velocity and potential temperature so eddy diffusivity and eddy viscosity are assumed to have the same values:  $K_z^\theta = K_z^u$  (Hourdin, 1992).

The eddy viscosity is computed based on a mixing length model, where  $K_z^u$  is proportional to the vertical shear and the  
440 square of a “mixing length”  $l$ . The mixing length is the mean distance over which the quantity  $q$  becomes fully mixed by the turbulence. In addition, the eddy viscosity is proportional to a nonlinear term that measures the net production of turbulence by buoyancy and velocity shear instabilities.

$$K_z^u = l(z)^2 \left\| \frac{\partial \mathbf{u}}{\partial z} \right\| \sqrt{1 - \frac{Ri}{Ri_c}}. \quad (22)$$

Computing the eddy viscosity  $K_z^u$  therefore requires the vertical gradient of the horizontal velocity (the shear), the gradient  
445 Richardson’s number ( $Ri$ ), the critical Richardson’s number ( $Ri_c = 0.4$ ) and the mixing length  $l$ . To ensure stability, the model sets a lower bound on the vertical shear  $\|\partial_z \mathbf{u}\|^2 = 10^{-3} \text{ s}^{-1}$ . Note that all these quantities can be diagnosed from the prognostic variables provided by the dynamics.

The mixing length is modeled by

$$l(z) = \left( \lambda^{-1} + \frac{1}{\kappa(z + z_0)} \right)^{-1}, \quad (23)$$

450 where  $\kappa$  is the Von Karman constant and  $\lambda$  is the minimum mixing length. We set  $\kappa = 0.4$  and  $\lambda = 100 \text{ m}$ .

The gradient Richardson’s number (Hourdin, 1992) is approximated as,

$$Ri = \frac{\frac{g}{\theta} \frac{\partial \theta}{\partial z}}{\left\| \frac{\partial \mathbf{u}}{\partial z} \right\|^2}, \quad (24)$$

the ratio between the buoyant production and consumption of turbulence (represented by the numerator) and the wind shear  
production of turbulence.  $Ri_c$  is a dynamic stability criteria: when  $Ri < Ri_c$ , there is a net production of turbulence. The  
455 critical Richardson number is set to  $Ri_c = 0.4$ . When  $Ri > Ri_c$  a minimum eddy viscosity is imposed (Hourdin, 1992),

$$K_z^u = l(z) \sqrt{e_{min}}. \quad (25)$$

where  $e_{min}$  is interpreted as a lower bound on the TKE. The minimum TKE is set to the small value  $e_{min} = 10^{-16} \text{ m}^2 \text{ s}^{-2}$  to avoid spurious vertical diffusion in inactive regions. The maximum diffusivity  $K_{max}^u$  is set to  $1 \text{ m}^2 \text{ s}^{-1}$ .

The physics model for vertical diffusion is therefore simply given by Fick’s second law,

$$460 \quad \frac{\partial \mathbf{u}}{\partial t} = \frac{\partial}{\partial \zeta} \left( K_z^u \frac{\partial \mathbf{u}}{\partial \zeta} \right), \quad (26)$$

where the eddy viscosity  $K_z^u$  is computed using the mixing length model (22) and  $\zeta$  is a floating vertical coordinate. As mentioned above, the diffusion equation dissipates resolved kinetic energy  $K$  provided by the dynamics step at the rate  $\epsilon$  and diffuses this kinetic energy vertically.

The SGS physics model for heat includes a radiative flux term and a source term  $\epsilon$  due to heating (due to the dissipation of TKE and, indirectly, from the dissipation of  $K$ ) in addition to the turbulent diffusion term,

$$h_\theta \frac{\partial \theta}{\partial t} = \frac{\partial}{\partial \zeta} \left( h_\theta K_z^\theta \frac{\partial \theta}{\partial \zeta} \right) - \frac{\partial F_{rad}}{\partial \zeta} + \epsilon, \quad (27)$$

where  $\theta$  is the potential temperature,  $h$  is the enthalpy,  $h_\theta = \partial h / \partial \theta$ . Recall that we assume that  $K_z^\theta = K_z^u$ .

The equation for resolved kinetic energy  $K = 1/2 \|\mathbf{u}\|^2$  is derived from the prognostic equation for velocity (26) by taking its inner product with  $\mathbf{u}$  and rearranging,

$$\frac{\partial K}{\partial t} + \frac{1}{\rho} \frac{\partial \mathbf{F}_K}{\partial \zeta} = -\epsilon \quad (28)$$

where  $\mathbf{F}_K = \mathbf{u} \cdot (\frac{1}{\rho} F_u \hat{\mathbf{z}})$  is the vertical flux of  $K$ . This provides an expression for the TKE dissipated to heat,  $\epsilon$ , which is included in the turbulent diffusion equation for potential temperature (28),

$$\epsilon = -\left(\frac{1}{\rho} F_u \hat{\mathbf{z}}\right) \cdot \frac{\partial \mathbf{u}}{\partial z} = K_z^u \left\| \frac{\partial \mathbf{u}}{\partial z} \right\|^2. \quad (29)$$

Since our turbulence model is only a first order closure approximation, there is no need for a model equation for  $\epsilon$ : it is diagnosed directly from the prognostic variables. It is assumed that the part of the resolved kinetic energy that is dissipated at rate  $\epsilon$  is instantaneously converted to heat (rather than first being converted to TKE). The heat equation (27) must therefore include a corresponding source term  $\epsilon$ .

In contrast, in the second-order  $k$ - $\epsilon$  model, the eddy viscosity  $K_z^u \propto k^2 / \epsilon$ , where  $k$  is the (unresolved) small scale TKE.  $K_z^u$  therefore depends on two unresolved quantities that must be modeled. They are computed by solving two coupled time-dependent model equations for their tendencies.

With a block cell vertical discretization, as explained in section Section 2.5.1, the tendency equation for momentum, discretized at cell layer center  $k$  is

$$D_t \mathbf{u}_k = -\frac{1}{\rho_k} \frac{\mathbf{F}_{k+1/2} - \mathbf{F}_{k-1/2}}{\Delta z_k}, \quad (30)$$

$$\mathbf{F}_{k+1/2} = \left( K^u \frac{\partial u}{\partial z} \right)_{k+1/2} = K_{k+1/2}^u \frac{u_{k+1} - u_k}{\frac{1}{2}(\Delta z_{k+1} + \Delta z_k)} \quad (31)$$

$$\mathbf{F}_{k-1/2} = \left( K^u \frac{\partial u}{\partial z} \right)_{k-1/2} = K_{k-1/2}^u \frac{u_k - u_{k-1}}{\frac{1}{2}(\Delta z_k + \Delta z_{k-1})}, \quad (32)$$

where  $D_t \mathbf{u}_k$  is the material derivative of momentum and  $\mathbf{F}_{k\pm 1/2}$  are the vertical turbulent momentum fluxes at the upper and lower interfaces  $k \pm 1/2$ . The tendency equation for heat follows the same scheme as the momentum equation,

$$h_\theta D_t \theta_k = -\frac{1}{\rho_k} \frac{\mathbf{F}_{k+1/2} - \mathbf{F}_{k-1/2}}{\Delta z_k} \quad (33)$$

$$F_{\theta, k+1/2} = \left( K^u \frac{\partial \theta}{\partial z} \right)_{k+1/2} = K_{k+1/2}^u \frac{\theta_{k+1} - \theta_k}{\frac{1}{2}(\Delta z_{k+1} + \Delta z_k)} \quad (34)$$

$$490 \quad F_{\theta, k-1/2} = \left( K^u \frac{\partial \theta}{\partial z} \right)_{k-1/2} = K_{k-1/2}^u \frac{\theta_k - \theta_{k-1}}{\frac{1}{2}(\Delta z_k + \Delta z_{k-1})}, \quad (35)$$

where the turbulent dissipation rate  $\epsilon$  is neglected and  $\mathbf{F}$  is the total heat flux, incorporating both the turbulent and radiative heat flux. These equations are completed by Neumann (flux) boundary conditions at the bottom and top of each vertical column. The flux at the top of the atmosphere is assumed to be zero for both velocity and potential temperature,  $F_{u,N} = F_{\theta,N} = 0$ , while the fluxes at the ground,  $F_{u,0}, F_{\theta,0}$  are provided by the surface flux parameterization scheme discussed in the following section.

The radiative heat flux is computed by the radiative transfer scheme and is an input to the turbulence model. During a time step the inputs to the model are the surface temperature and surface heat flux at the surface boundary, while the outputs of the model are the tendencies for velocity and potential temperature due to the parameterized SGS processes.

### 2.3.2 Surface flux scheme

500 The surface heat and momentum drag flux are computed using the inputs of  $z, \theta$  and  $u$ , at the lowest (surface) layer center of the column ( $k = 1$ ). The parameterization for the fluxes are the bulk formulae of Louis (1979), which are based on the Monin–Obukhov similarity theory for boundary layer turbulence that describes vertical profiles of velocity and potential temperature as a function of height  $z$  and the Obukhov length  $L$ ,  $z/L$ . The flux model uses the following parameters, derived by Louis (1979):

$$\begin{aligned}
 a &= \frac{\kappa}{\log(z/z_0)} & c^* &= 2bC^* a^2 \left( \frac{z}{z_0} \right)^{1/2} \\
 b &= 4.7 & f^* &= 1 - \frac{2b Ri_B}{1 + c^* \sqrt{-Ri_B}} && \text{(if } Ri_B < 0) \\
 505 \quad C^u &= 7.4 & f^* &= \frac{1}{(1 + b Ri_B)^2} && \text{(if } Ri_B > 0) \\
 C^\theta &= 5.3 & C_D^u &= a^2 u f^u \\
 Ri_B &= \frac{gz(\theta - \theta_0)}{\theta(u^2 + e_{min})} & C_D^\theta &= \frac{a^2 u}{R} f^\theta \\
 R &= 0.74,
 \end{aligned}$$

where  $z_0 = 0.1$  m is roughness length,  $\theta_0$  is the potential temperature at  $z_0$ ,  $Ri_B$  is the bulk Richardson's number,  $\kappa = 0.4$  is the Von Karman constant. The exponent \* replaces  $u$  or  $\theta$  and  $C_D^\theta$  are drag coefficients for velocity and potential temperature.  $a$  represents the drag coefficient in the neutral surface condition case, while the coefficient calculated for  $Ri_B < 0$  and  $Ri_B > 0$  models the drag coefficients in the unstable and stable cases respectively.  $R$  is an empirical parameter that relates  $C_D^\theta$  to  $C_D^u$ .

510 The surface fluxes are therefore computed as surface drags using the drag coefficients computed above,

$$\mathbf{F}_u = -\rho C_D^u \mathbf{u}, \quad (36)$$

$$F_\theta = -\rho C_D^\theta (\theta - \theta_0). \quad (37)$$

### 2.3.3 Soil

The inclusion of a multi-layer soil model is rare in simple physics models. However, our model includes a soil column which  
 515 stores and releases heat over a wide range of time scales in order to provide more accurate and realistic conditions at the surface  
 boundary. In this model the only prognostic variable of the soil is its depth-dependent temperature  $T_s(z, t)$ , with  $z < 0$ . The  
 heat flux in the soil is

$$F_s = -k \frac{\partial T_s}{\partial z} \quad (38)$$

where  $k$  is the thermal conductivity in  $\text{W} [\text{K m}]^{-1}$ .

520 From Fick's second law the temperature tendency in the soil is given by the diffusion equation (Hourdin, 1992),

$$\frac{\partial T_s}{\partial t} = -\frac{1}{I} \frac{\partial F_s}{\partial z} = \frac{k}{I} \frac{\partial^2 T_s}{\partial z^2}, \quad (39)$$

where  $k$  is the thermal conductivity and the thermal inertia  $I = 3000 \text{ J m}^2 \text{ K}^{-1} \text{ s}^{-1/2}$ .

The soil is discretized by  $N_S = 10$  layers, where the heat fluxes are computed at layer interfaces  $l = -N_S, \dots, 0$ , where  
 $l = 0$  is the surface. The interfaces are located at generalized depths

$$525 \zeta'_l = \frac{\alpha^l - 1}{\alpha - 1} \sqrt{T}, \quad (40)$$

where the time scale  $T = 2000 \text{ s}/\pi$  and exponent  $\alpha = 2$  are model parameters. Depth is therefore measured as in terms of time,  
 where deep layers correspond to increasingly slow heat diffusion time scales. Including more vertical layers add more slow  
 time scales to heat diffusion in the soil column. Table 2 shows the time scales corresponding to each soil layer for the  $N_S = 10$   
 soil layer case considered in this paper.

530 The first interface below the surface is ( $\zeta'_1 = \sqrt{T}$ ) and it includes the damping depth of the diurnal wave. The damping depth  
 is the depth of a wave of period  $P$  whose amplitude is reduced by  $e$  (Arya, 1988). More generally, the depth of penetration of  
 a wave of period  $P$ , in days, is  $\sqrt{P}$  (Hourdin, 1992). More layers included in the soil model allows for the release of energy at  
 more (longer) time scales, for example a diurnal, monthly and annual time scales.

Fluxes at interface  $l$  are computed by:

$$535 F_{s,l} = I \frac{T_{s,l+1/2} - T_{s,l-1/2}}{\frac{1}{2}(\Delta \zeta'_{l+1/2} + \Delta \zeta'_{l-1/2})}, \quad (41)$$

where  $\Delta \zeta'_{l+1/2} = \zeta'_{l+1} - \zeta'_l$ . Therefore, the soil temperature tendency of soil layer  $l + 1/2$  is defined by

$$\frac{\partial T_s}{\partial t} = -\frac{1}{I} \frac{F_{s,l} - F_{s,l-1}}{\zeta'_l - \zeta'_{l-1}}. \quad (42)$$

Layer	Period	Depth [m]
1	5.6 hours	0.11
2	2.1 days	0.33
3	11 days	0.76
4	52 days	1.6
5	220 days	3.4
6	2.5 years	6.9
7	10 years	14
8	41 years	28
9	170 years	56
10	660 years	110

**Table 2.** The time periods of each soil layer and their equivalent depth. 10 soil layers is sufficient for climate simulations of up to about 1000 years. The calculated depth in the table uses the heat capacity  $C_p = 2.2 \times 10^6 \text{ J m}^{-2} \text{ K}^{-1}$  and thermal conductivity  $\lambda = 4.09 \text{ J s}^{-1} \text{ m}^{-2} \text{ K}^{-1}$ .

If there are  $L_s$  layers, the Neumann boundary conditions for the soil column are

$$F_{s,0} = F_r + F_H, \quad (\text{Flux at ground boundary, } l = 0)$$

$$540 \quad F_{s,L_s} = 0, \quad (\text{Flux of bottom soil interface } l = L_s)$$

where  $F_r$  is the surface radiative flux and  $F_H$  is the surface heat flux.

### 2.3.4 Dry Convective Adjustment

Dry convection must be parameterized because the dynamics makes the hydrostatic approximation. The vertical turbulence model only simulates turbulent diffusion, not convection. It could therefore produce an unstable vertical temperature stratification, characterized by  $\partial\theta/\partial z < 0$  (Hourdin, 1992). The dry convective adjustment scheme of the physics model mitigates any instability by instantaneously relaxing the temperature to an adiabatic profile.

A layer is unstable if its potential temperature is greater than that of the layers above. The convection parameterization scheme checks each column to see if a layer is unstable. If a particular layer of the one-dimensional vertical column is unstable, local mixing is applied. This local mixing is modeled by a temperature relaxation to the mass weighted temperature average of the unstable layers. This scheme also takes into account the transport of momentum that occurs with convection by mixing the momentum in the unstable layers. For each unstable layer in a column only a proportion  $\alpha$  of the cell is mixed, where

$$550 \quad \alpha = \frac{\int |\bar{\theta} - \theta| dp}{\int \theta dp}, \quad (43)$$

and  $\alpha < 0$ , which is always verified (Hourdin, 1992).

## 2.4 Physics package usage, input and output

- 555 The vertical physics model is intended to be coupled with a dynamical core. This coupling is usually done via a split step method, where the “dynamics” and “physics” components take alternate times steps. The prognostic variables of the physics package are temperature, zonal velocity and meridional velocity. When a physics step is taken, the package outputs the tendencies of the prognostic variables. Note that each of the the physics sub-models (radiation, turbulent diffusion, dry convective adjustment, diurnal cycle) can be turned on or off separately.
- 560 One of the major objectives of the package is its versatility in modeling different planets. In order to accommodate this goal, the package initialization allows users to read in input parameters to tailor the simulation to the desired planet. Beyond these parameters, calls to initialization routines set up the logistics of the grid.

## 2.5 Numerical integration and boundary coupling

### 2.5.1 Time integration

- 565 To solve the system of differential equations at the next time step a numerical integration method is employed. The explicit Euler method is a first-order method commonly used to numerically integrate a system of differential equations. Given an autonomous system of ODEs,

$$\frac{d\mathbf{S}}{dt} = \mathbf{F}(\mathbf{S}(t)), \quad (44)$$

- where  $\mathbf{F}(\mathbf{S}(t))$  is called the “tendency”. The stencil of the Explicit Euler method is given by the linear Taylor series approximation of  $\mathbf{S}(t^*) = \mathbf{S}(t + \tau) + O(\tau^2)$
- 570

$$\mathbf{S}(t^*) = \mathbf{S}_t + \tau \mathbf{F}(\mathbf{S}_t) \quad (45)$$

where:

- $t$  is the current time
- $\tau$  is the time step (assumed fixed)
- 575 –  $t^* = t + \tau$  is the time at the next discrete time
- $\mathbf{S}_t$  is the numerical approximation of  $\mathbf{S}(t)$ ,  $\mathbf{S}_t \approx \mathbf{S}(t)$ .

- A variety of time integration methods have been developed from the Explicit Euler method by making different approximations for the tendency of  $\mathbf{S}$ ,  $\mathbf{F}(\mathbf{S})$ , (e.g. Runge-Kutta schemes). These methods differ in their order of accuracy and numerical stability properties. In the Explicit Euler method the tendency is simply approximated as  $\mathbf{F}(\mathbf{S}_t)$ , where the values of  $\mathbf{S}$  are at time  $t$ . The implicit Euler method improves numerical stability by using the tendency for  $\mathbf{S}$  at the the next time step ( $\mathbf{F}(\mathbf{S}_{t^*})$ ). This requires more computation since a linear system must be solved at each time step, in general. However, Implicit Euler has a much wider stable domain compared to the Explicit Euler method, allowing for a larger time step and increasing its desirability. The radiation model uses Explicit Euler, while the soil and turbulence models use Implicit Euler.
- 580

## 2.5.2 Boundary coupling

585 Since the sub-components of the physics are air and soil, it is essential to specify how they are coupled in the time integration scheme. The air and soil columns are coupled via their boundaries, which is the horizontal interface between the soil and air (i.e., the ground), and the boundary conditions need to be taken into consideration and coupled when evaluating the tendencies of the two components. The simplest boundary coupling is explicit, and the boundary conditions are evaluated at time  $t$  from the previous state. Therefore, the time integration equation includes the boundary conditions  $\mathbf{q}_t$ ,

$$590 \mathbf{S}_{t^*} = \mathbf{S}_t + \tau \mathbf{F}(\mathbf{S}_t, \mathbf{q}_t). \quad (46)$$

Since the air and soil are strongly coupled, coupling the boundary conditions implicitly is desirable for improved stability. (Note that both the soil and air physics strongly affect temperature.) Therefore, the boundary conditions are evaluated at time  $t^*$ . The tendency is approximated as

$$\mathbf{F}(\mathbf{S}(t), \mathbf{q}(t)) \approx \mathbf{F}(\mathbf{S}_t, \mathbf{S}_{t^*}, \mathbf{q}_t, \mathbf{q}_{t^*}) \quad (47)$$

595

$$\mathbf{S}_{t^*} = \mathbf{S}_t + \tau \mathbf{F}(\mathbf{S}_t, \mathbf{q}_t) + \frac{\partial \mathbf{S}_{t^*}}{\partial \mathbf{q}_{t^*}} (\mathbf{q}_{t^*} - \mathbf{q}_t), \quad (48)$$

where  $\partial \mathbf{S}_{t^*} / \partial \mathbf{q}_{t^*}$  represents the dependence of  $\mathbf{S}_{t^*}$  on the boundary conditions at the new time  $t^*$ .

## 2.6 Spatial discretization

### 2.5.1 Spatial discretization

600 The physics package models the effects of the small scale unresolved physics on each 1D vertical column on the sphere, taking the current state of the prognostic dynamical variables as inputs. The vertical discretization is a block cell discretization, with all prognostic variables located at the center of each layer cell, while the fluxes are located at the interfaces between each layer. Each column has  $N$  layers, which is an input parameter to the package from the dynamics. There are a total of  $N + 1$  interfaces, where the surface (ground) interface has index 0 and top interface (top of atmosphere) has index  $N$ . The soil column  
605 is considered separately, with negative indices. With the chosen floating vertical coordinates, the height of each cell layer ( $\Delta z_k$ ) changes over time. Technical details are provided in A.

## 2.6 Limitations, Decisions and Possible Extensions

The simple dry physics package makes approximations to ensure it is relatively simple, stable and easy to use and understand. However, these choices necessarily mean the physics is idealized and not sufficiently realistic for many applications.

610 First, a dry climate is assumed by the package which neglects condensible substances (e.g., water or methane) on the atmosphere. The lack of moisture is a major limitation, especially for planets with condensible substances that have a major effect

on the atmosphere, like Earth. However, assuming a dry climate removes the added complexity of the effects of condensible substances and makes the physics much simpler. Due to this limitation, we cannot expect accurate results when modeling Earth. For example, the temperature of the surface temperature should be much higher than that of Earth. This is due to the fact  
615 that the lapse rate of the simulation is constrained to be close to the dry adiabatic lapse rate, to keep a physically consistent dry model, while the lapse rate for Earth is closer to the moist lapse rate.

Secondly, the surface flux parameterization in the physics package was created empirically using Earth observation data, which includes moisture. Therefore the scheme may not be suitable for modeling dry planets and might require tuning when modeling planets whose condensible substances are not water.

620 Finally, the current radiation parameterization uses only two frequency bands: shortwave (visible) and longwave (infrared). In general, radiation models are expensive, and therefore having only two frequency bands keeps the cpu time per step minimal. However, with only two radiation bands, when modeling Earth, the temperature will not be accurate in the stratosphere as UV light has a major effect on the temperature. Nevertheless, unlike for moisture, it is relatively simple to include additional radiation bands.

625 Adding a third absorption band for UV light would improve the realism of the vertical temperature profile in the stratosphere, producing the expected trend of an increase in temperature with height. However, this addition would increase the computational cost of the radiation step.

### 3 Configuration and Numerical Implementation

The simple dry physics package needs to be coupled with a dynamical core to simulate the atmospheric general circulation  
630 of a planet. In this section we describe the WAVETRISK dynamical core Kevlahan and Dubos (2019b) used to evaluate the characteristics of the physics package, the configuration of the physics-dynamics coupling and its numerical implementation. We also present the base simulation of the Held and Suarez (1994) dry physics model, which is to be used for future comparison of the simple dry physics package.

#### 3.1 WAVETRISK dynamical core

635 Since we want to better understand the need for scale-aware physics, and how dynamic adaptivity combines with a physics package, we use the WAVETRISK dynamical core. WAVETRISK is a global three-dimensional dynamically adaptive hydrostatic dynamical core that can be run in both adaptive and non-adaptive modes (as well as in atmosphere or ocean configurations). This allows us to directly compare equivalent adaptive and non-adaptive runs. WAVETRISK utilizes a hexagonal-triangular C-grid with the TRiSK horizontal discretization scheme, which is well known for its mimetic properties and stability.

640 Dynamic horizontal grid adaptivity is implemented using a multiscale wavelet approach with user-specified minimum (coarsest) and maximum (finest) resolutions. Nodes and edges are added or removed at each scale as necessary to achieve a user-specified relative error tolerance for each prognostic variable (i.e., pseudo-density  $\mu = \rho_0 \Delta z$ , mass-weighted potential temper-

ature  $\Phi = \mu\theta$ , and edge velocities  $u, v, w$ ). A node/edge is retained if it is retained in any vertical layer. The computational grid is adapted after each full time step as follows:

- 645 1. Compute wavelet coefficients at each horizontal position/vertical layer/horizontal resolution scale for all prognostic atmosphere variables.
2. If a wavelet coefficient is above the dimensional tolerance threshold for any prognostic variable at any vertical layer, keep the associated grid point. If not, delete it.
3. Add to the active grid the nearest neighbour grid points at the same scale and at the finer scale. This allows for a local  
650 scale-dependent CFL criterion  $u\Delta t/\Delta x \leq 1$  and accounts for quadratic nonlinearities (which can generate scales twice as small in a single time step).
4. Interpolate all prognostic variables (including soil temperature) onto the new adapted grid.

This process ensures that the grid adaptation algorithm conserves mass and various mimetic properties. The resulting adaptive grid is a set of columns of varying cross-section. WAVETRISK may be run either adaptively with a range of horizontal resolu-  
655 tions, or non-adaptively with a fixed horizontal grid resolution. Full details on the WAVETRISK model are given in Kevlahan and Dubos (2019a).

### 3.2 Model configurations

Time discretization uses an explicit low storage fourth-order Runge–Kutta step for WAVETRISK and an implicit Euler step for the physics package. Both the dynamical core and the physics package have the same time step, with WAVETRISK determining  
660 the time step and supplying it to the physics. The adaptive simulation uses the time step determined by the finest resolution.

We use horizontal bi-Laplacian hyperdiffusion for vorticity  $\nabla \times \mathbf{u}$ , velocity divergence  $\nabla \cdot \mathbf{u}$  and scalars to reduce grid scale noise. The hyperviscosity  $\nu_4$  is defined non-dimensionally as a proportion of the maximum stable value for the given time step  $\Delta t$  and minimum average grid size  $\Delta x_{\min}$  ( $\Delta t$  is based on  $\Delta x_{\min}$ ). The maximum stable viscosity is the analytical value for the hexagonal/pentagonal C-grid on the plane, modified with empirical correction factors for the irregular multiscale hexagonal  
665 C-grid on the sphere. (The empirical corrections are conservative by 15% to 33%, and are based on Gershgorin circle theorem estimates evaluated on the actual multiscale grids.) Note that the TRisK discretization (Ringler et al., 2010) is stable without horizontal diffusion on a fixed resolution grid, but there is some grid scale noise.

WAVETRISK uses Lagrangian (floating) vertical coordinates with periodic conservative remapping of the prognostic variables to the initial hybrid pressure grid. Note that vertical remapping introduces some vertical diffusion. The data structure combines  
670 the atmosphere layers and soil layers into a single vertical column, but only the atmosphere layers require remapping. All simulations have 30 hybrid pressure layers, with the top of the atmosphere at 225 Pa. The  $A, B$  hybrid pressure coefficients are given in Ullrich et al. (2012) Table XVIII. Layer 6 is at 850 hPa and layer 12 is at 533 hPa. There is no orography. There are 10 soil layers for all simulations.

Run label	Resolution [ $^{\circ}$ ]	Resolution [km]	Physics Model	Seasons
HS 2.0	$2^{\circ}$	240	Held and Suarez	no
UNIF 2.0 NS	$2^{\circ}$	240	Simple physics	no
UNIF 2.0	$2^{\circ}$	240	Simple physics	yes
UNIF 1.0	$1^{\circ}$	120	Simple physics	yes
UNIF 0.5	$0.5^{\circ}$	60	Simple physics	yes
ADAPT 0.5	$2.0^{\circ}, 1^{\circ}, 0.5^{\circ}$	240, 120, 60	Simple physics	yes
ADAPT 0.25	$2.0^{\circ}, 1^{\circ}, 0.5^{\circ}, 0.25^{\circ}$	240, 120, 60, 30	Simple physics	yes

**Table 3.** Parameters for the simulation runs discussed in the following sections. All runs use 30 vertical pressure layers. All simple physics runs also include 10 soil layers. All simulations, except ADAPT 0.25, are run for 5 years, with data saved every 5 days. ADAPT 0.25 is a special case that is restarted from UNIF 2.0 with 8 times higher resolution and then run for an additional 100 days. All adaptive simulation use a relative tolerance of  $\varepsilon = 2.5\%$ , except ADAPT 0.25 which uses 3%. The relative tolerance  $\varepsilon$  determines the local horizontal grid resolution at each time step.

The physics uses Earth astronomical values and boundary drag parameterizations, including seasons (see Table 1). The initial conditions for prognostic variables are based on an isothermal temperature profile of 250 K and zero velocity. While it would be more realistic to have an initial temperature that depends on latitude, a horizontally uniform isothermal profile is a simple initial condition that has been used in Dynamical Core Intercomparison Projects (DCMIP) (e.g. Kent et al. (2014)) and the climate dynamics develops within a few days.

The reference resolution used to characterize the climatology of the WAVETRISK–simple physics coupling is a relatively coarse non-adaptive  $2^{\circ}$  ( $\sim 240$  km) simulation. A resolution of  $2^{\circ}$  is considered sufficient for coarse climate simulations.

The adaptive simulation uses a minimum resolution of  $2^{\circ}$  ( $\sim 240$  km) and a maximum resolution of  $0.5^{\circ}$  (60 km). This means that the maximum possible refinement is 4 times and the maximum grid compression is  $4^2 = 16$  (i.e., about 16 times faster than a non-adaptive simulation with the maximum resolution). The simulations are initialized at the coarsest  $2^{\circ}$  resolution and refined and coarsened after each time step with a relative error tolerance of 2.5% for based on the  $\ell_2$  norms for each vertical layers.

All simulations are run for 5 (Earth) years. This period includes two years for the means of the prognostic variables in all layers to converge to within about 2% for runs with seasons. The value of 2% was chosen (rather than a smaller value) since the climate variables have significant intrinsic variance due to turbulence. The basic parameters and labels for all runs discussed below are given in Table 3.

The climatology of the physics–dynamics coupled simulations is characterized by 5-year zonal first- and second-order statistics: mean temperature, mean zonal velocity, eddy kinetic energy, eddy heat flux temperature variance and eddy momentum flux. In addition, we include the vertical profile of temperature, averaged over the sphere and instantaneous horizontal

slices of temperature and vorticity. The results for the  $0.5^\circ$  adaptive simulation include a visualization of instantaneous three-dimensional vorticity isosurfaces, zonally averaged vertical velocity and energy spectrum results.

## 695 4 Results

This section presents and discusses results from the uniform and adaptive simulation runs summarized in Table 3. We begin in §4.1 by comparing the climatology from the Held–Suarez physics model (HS 2.0) with the climatology of simple physics without seasons (UNIF 2.0 NS). This provides a baseline to appreciate the new features provided by the more complex simple physics model. § 4.2 presents low resolution climatology for the simple physics with seasons (UNIF 2.0). These results form  
700 the basis for comparing with the high resolution uniform (UNIF 0.5) and adaptive (ADAPT) results in § 4.2. This section shows how the climatology and instantaneous prognostic fields change as the horizontal resolution is increased by a factor of 4; it also validates and characterizes the ability of the adaptive simulation to capture the climatology and energy spectra of the non-adaptive high resolution simulation. Finally, § 4.4 quantifies the computational performance of the adaptive runs ADAPT 0.5 and ADAPT 0.25 compared to equivalent uniform runs. Key metrics include the grid compression ratio, stability  
705 and the ability to restart from a uniform low resolution run at much higher adaptive resolution.

### 4.1 Held–Suarez (HS 2.0) compared to low resolution simple physics without seasons (UNIF 2.0 NS)

The Held–Suarez physics model (Held and Suarez, 1994) is the simplest dry physics model that can be coupled to dynamical cores and a standard benchmark used for comparison of other simplified physics models. Therefore our initial comparison for the simple dry physics package will be to this model which includes only a relaxation of temperature to a radiative equilibrium  
710 value and a layer dependent linear damping of velocities in the surface boundary layer. HS 2.0 is a non-adaptive WAVETRISK simulation, using the initial conditions of Jablonowski and Williamson 2006. Figure ?? presents the zonal statistics from HS 2.0.

It is important to note that, although it is a standard benchmark, and therefore an interesting comparison, the Held and Suarez physics model is fundamentally different from the simple physics model, and so we should not expect qualitatively  
715 or quantitatively similar statistics. In the Held and Suarez physics model temperature is relaxed exponentially to a specified latitude and height-dependent profile, based on Earth climatology, and Rayleigh friction damps velocity near the surface (i.e., for pressures greater than 700 hPa) with a 1 day relaxation time. There are no other physical processes represented and the physics does not directly modify the dynamics, except by through the temperature relaxation and boundary friction. In addition, the simple physics model includes diurnal radiation forcing and there is no diurnal scale in the Held & Suarez (HS) temperature  
720 relaxation (the relaxation time scale is about 40 days in the stratosphere).

It is helpful to begin by comparing the simple physics climatology without seasons to the most basic physics model of Held and Suarez (1994). To do this, we ran a 5 year WAVETRISK non-adaptive simulation coupled to simple physics without seasons (i.e., obliquity of  $0^\circ$ ). We refer to this run as UNIF 2.0 NS. (Note that Kevlahan and Dubos (2019a) found that the Held and Suarez results are relatively insensitive to resolution.)

725 The Held–Suarez and simple physics results shown in Figure 1 are broadly similar, although their structures differ in position, shape and intensity. The biggest differences are in the eddy kinetic energy (KE), which has a different zonal jet shape, and in the zonal velocity which has its highest velocity near the top of the atmosphere, rather than at a similar pressure as the highest eddy KE. Furthermore, while the eddy heat flux and temperature variance differs between the simple physics and the HS simulations, the overall structure of the two statistics are similar, with high values near the mid-latitudes and at a normalized  
730 pressure of  $\sim 0.85$ .

Figure 2 presents the temperature profile for the non-adaptive  $2^\circ$  low resolution simple physics simulation without seasons, compared to the International Standard Atmosphere (ISA) model profile and the equilibrium state of the HS model (Held and Suarez, 1994), explained in the previous section. The ISA is a standard temperature profile for Earth.

The simple physics profile, plotted in red, is spatially averaged over the sphere at each layer and temporally averaged over  
735 five years. The temperature profile decreases monotonically with height, without a well-defined tropopause. In comparison to the standard atmosphere and HS, the simple physics temperature profile has a significantly warmer surface and cooler upper stratosphere. A hotter surface is expected to the lack of moisture in the atmosphere, while the continued decrease in upper atmosphere temperature is due to the lack of a UV radiation absorption band in the stratosphere, as mentioned in section 2.6.

#### 4.2 Non-adaptive low resolution $2^\circ$ simulation climatology with seasons (UNIF 2.0)

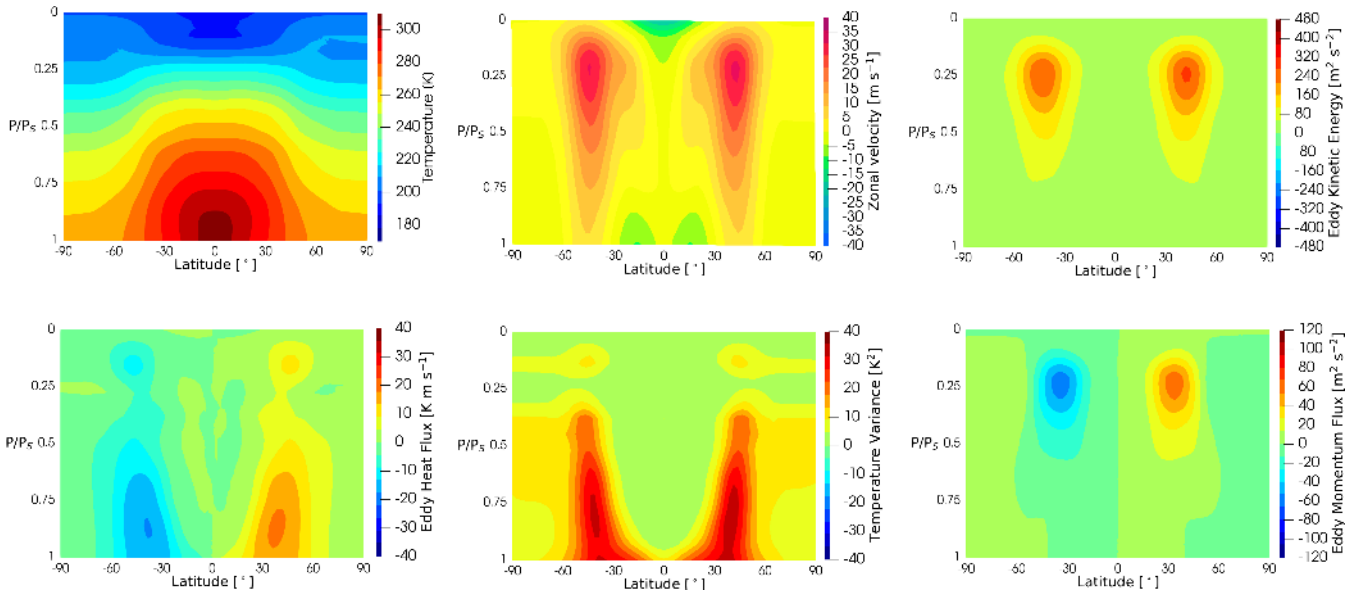
740 Figure 3 shows the 5 year seasonal zonal first- and second-order climatology statistics for UNIF 2.0. Unsurprisingly, the statistics are markedly different with seasons compared to the equivalent results without seasons shown in Figure 1. As pressure decreases with height, the temperature decreases, but there is also minimal zonal temperature variance near the top of the atmosphere. The large temperature variance at the poles is simply due to the effect of seasons. Furthermore, eddy KE has a zonal jet at the mid latitudes with a peak variance at  $P/P_S \sim 0.25$ . Overall, simple physics with seasons has qualitatively and  
745 quantitatively distinct climatology from Held–Suarez and Simple physics without seasons. Only the mean zonal temperature and high altitude peaks of eddy kinetic energy at  $\pm 40$  N/S and  $P/P_S = 0.25$  qualitatively similar.

An interesting feature of the simple physics with seasons climatology is the peaks in eddy KE, eddy momentum and heat flux at  $15^\circ$  N/S near the surface. This feature does not appear in the simple physics simulation without seasons shown in Figure 1. This suggests that seasonal radiation forcing greatly changes the climatology, both (unsurprisingly) at the poles, but also in the  
750 surface boundary layer near the equator. The Held–Suarez model cannot capture this effect.

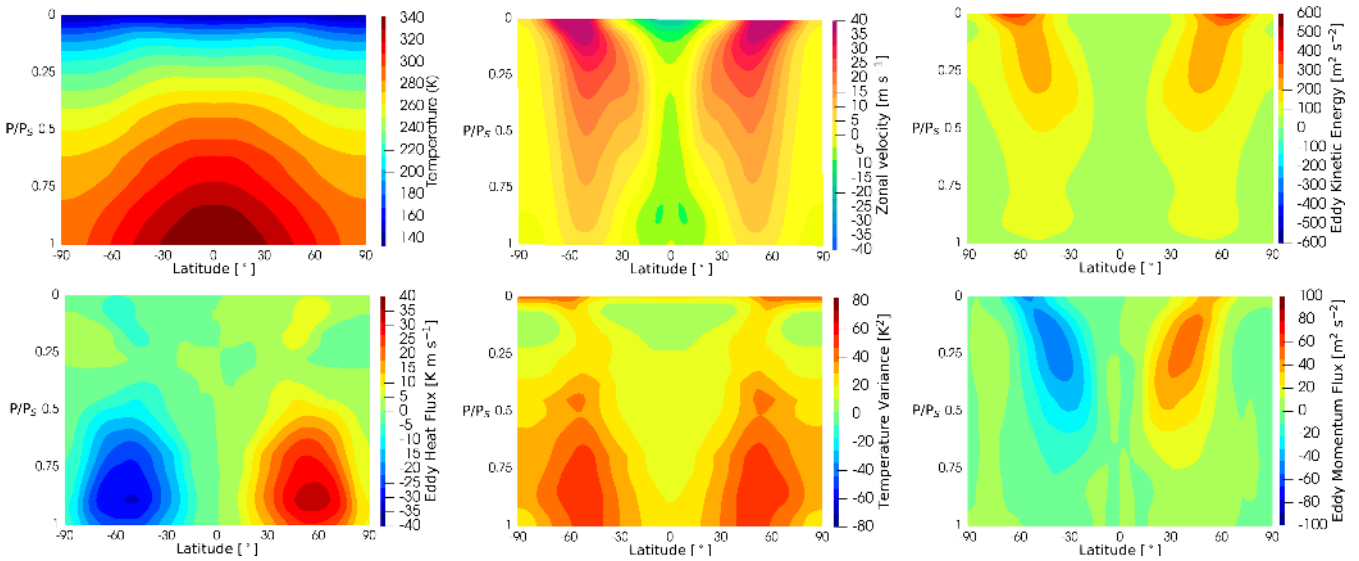
In the following section we present results for the high resolution non-adaptive (UNIF 0.5) and adaptive (ADAPT 0.5) runs. We assess the ability of the dynamically adaptive wavelet technique to capture important features of UNIF 0.5, and compare the climatology of the high resolution simulations with the low resolution UNIF 2.0 results discussed here.

#### 4.3 Comparison of adaptive (ADAPT 0.5) and uniform (UNIF 0.5) high resolution simulations

755 Dynamically adaptive GCMs have the potential to significantly improve accuracy and computational efficiency by adjusting the local horizontal grid resolution at each time step to ensure a given tolerance. In this section we investigate the key questions from the Introduction (Section 1) regarding the dynamically adaptive GCM. We focus on the adaptive physics-dynamics



(a) HS 2.0 climatology.



(b) UNIF 2.0 NS climatology (no seasons).

**Figure 1.** Comparison of the climatology of the zonal statistics for the low resolution HS 2.0 and UNIF 2.0 NS simulations. All statistics were averaged every 5 days over 5 years. Although the statistics are broadly similar, their features differ in position, shape and intensity.

coupling’s stability, ability to capture small-scale structure and the complete energy spectra. Our main way of validating ADAPT 0.5 is to compare its results directly with an equivalent uniform high resolution simulation, UNIF 0.5. We also compare with the low resolution UNIF 2.0 results presented in the previous section.

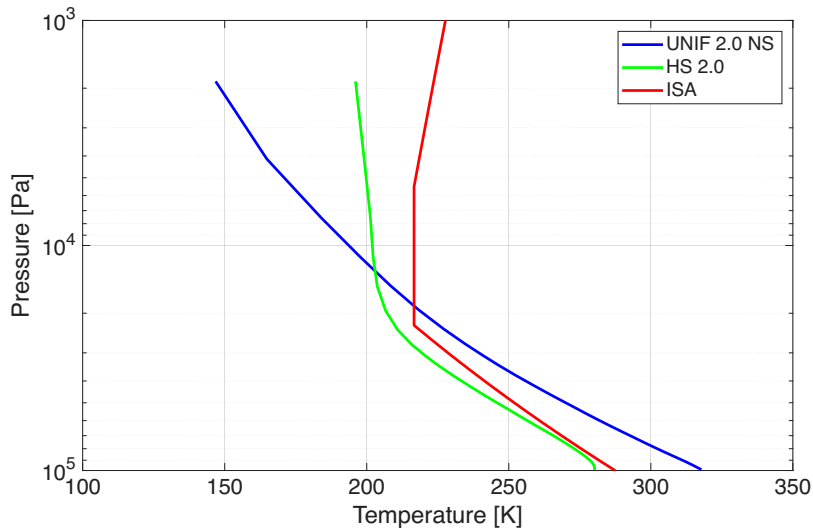
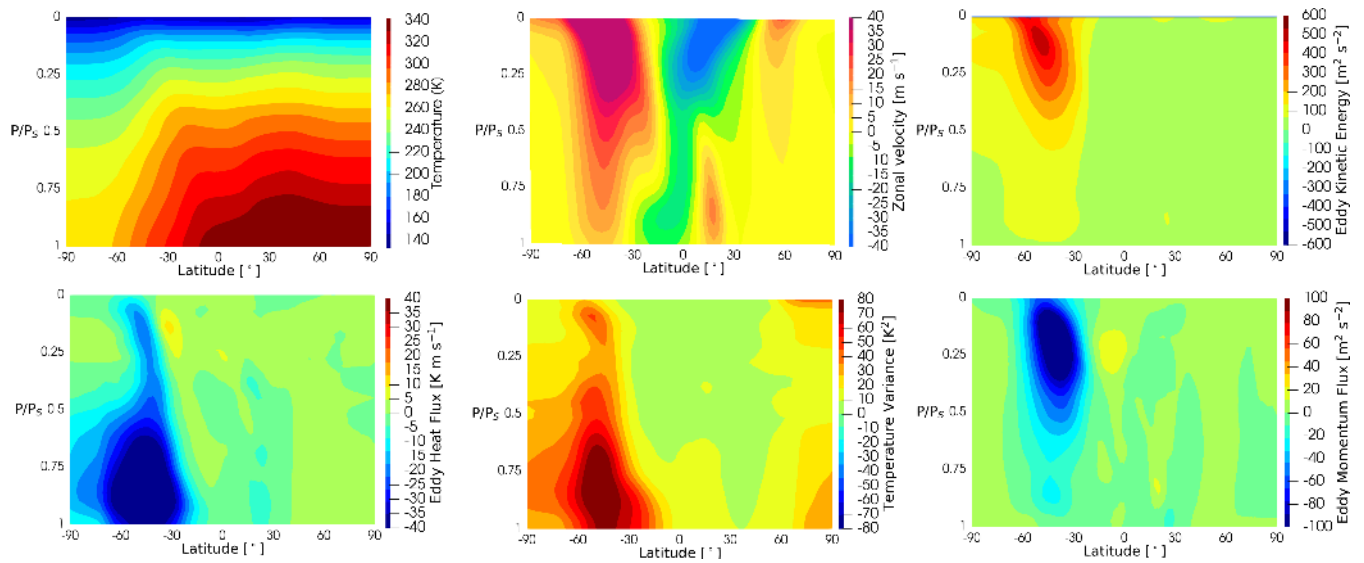


**Figure 2.** Temperature profile averaged over five years from the UNIF 2.0 NS run (simple physics with no seasons) and the HS 2.0 run (Held and Suarez physics). The figure also displays the International Standard Atmosphere temperature profile (ISA).

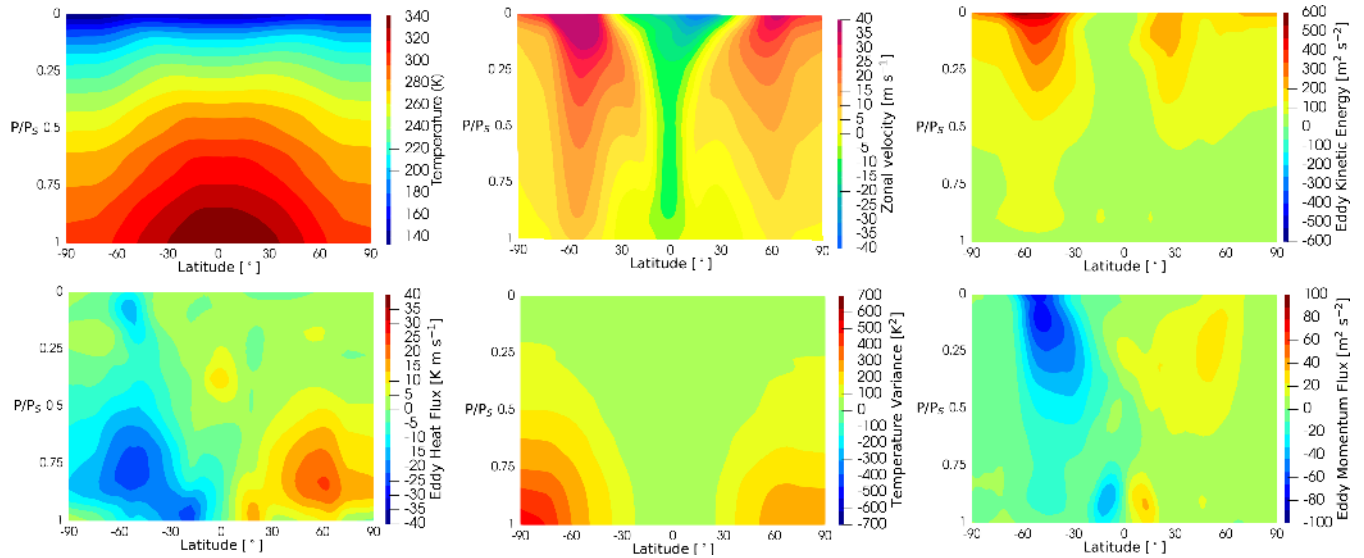
The simple physics package coupled to WAVETRISK-ATMOSPHERE is run adaptively with a coarsest average grid resolution of  $2^\circ$  and a finest average grid resolution of  $0.5^\circ$  (i.e., local horizontal grid refinement of up to 16 times). There are 30 vertical atmosphere layers and 10 soil layers. The relative error tolerance is 2.5% for all prognostic variables with the  $\ell_2$  tolerance normalization determined separately for each atmosphere layer. The grid is adapted explicitly only on the prognostic dynamical variables, not on the physics (e.g., tendencies of the vertical diffusion or radiation sub-models). Simulations are run for 5 years and climatology statistics are computed over the full five years. The adaptive results ADAPT 0.5 are compared with an equivalent non-adaptive run UNIF 0.5.

### 4.3.1 High resolution climatology statistics

The high resolution first- and second-order climatology statistics of ADAPT 0.5 and UNIF 0.5 for summer and fall are compared in Figures 4 and 5. The adaptive and non-adaptive results are qualitatively very similar, although the extrema of the second-order statistics are slightly smaller in ADAPT 0.5. However, a comparison with the low resolution results shown in Figures 3 shows that the high resolution climatology statistics are not qualitatively very different from the low resolution statistics. We will therefore examine the *differences* between the ADAPT 0.5 and UNIF 0.5 climatology statistics. We also discuss instantaneous temperature and vorticity fields as well as the rotational and divergent components of the energy spectra to get a complete statistical, dynamical and spectral understanding of the climate model. These more sensitive diagnostics provide different measures of the differences between the adaptive and uniform simulations, as well as how the low and high resolution results differ.



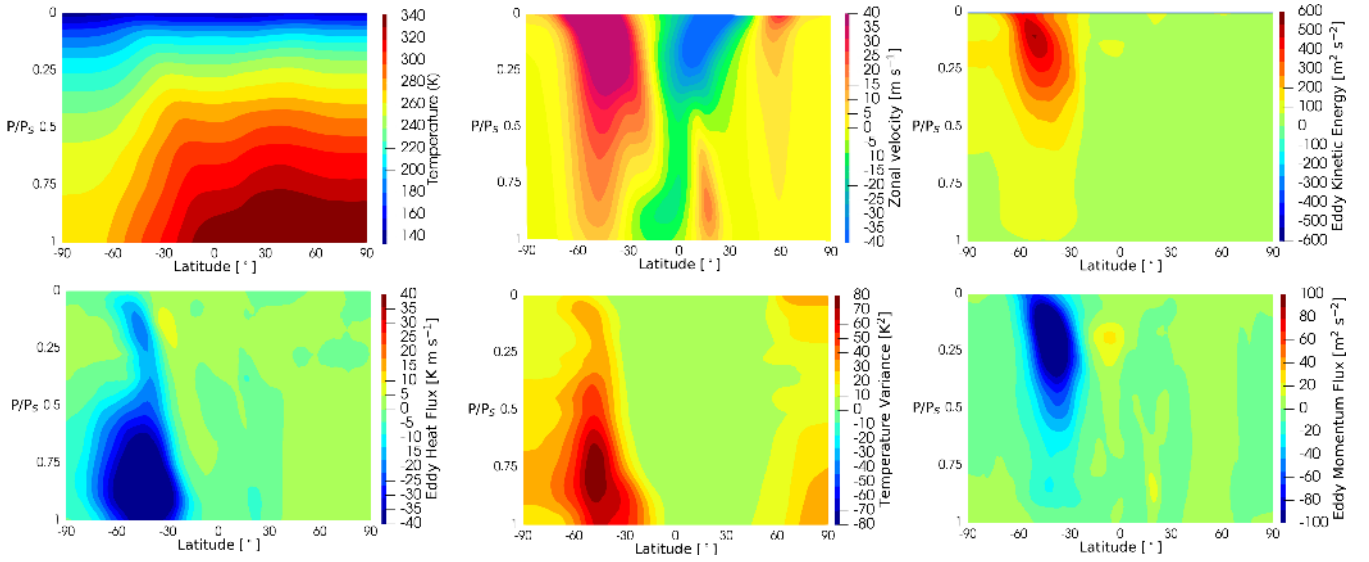
(a) Summer climatology: UNIF 2.0.



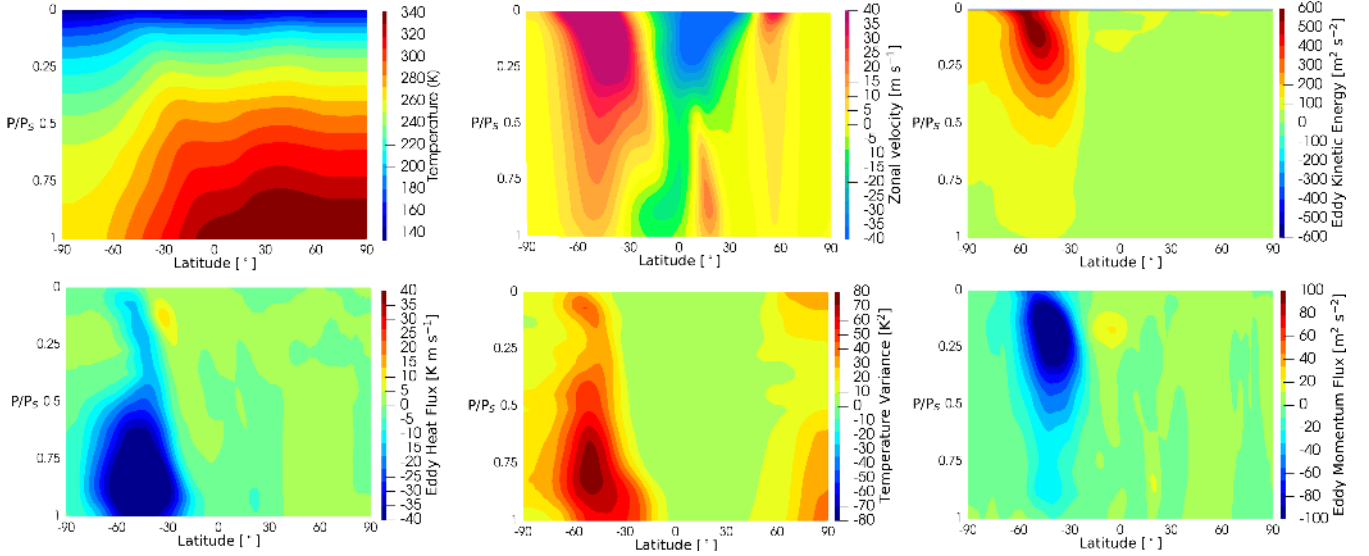
(b) Fall Climatology: UNIF 2.0.

**Figure 3.** Summer and fall zonal climatology statistics of the low resolution UNIF 2.0 simulation. The effect of seasonality is very strong. Extreme values are larger, there is strong N/S asymmetry and more pronounced fine scale structure compared the equivalent non-seasonal simple physics climatology shown in Figure 1.

Figure 6 shows the differences in climatology statistics between ADAPT 0.5 and UNIF 0.5 computed over the final 3 years of the simulations. These differences are greatest at high latitudes, where the adaptive grid is coarsest, especially around the



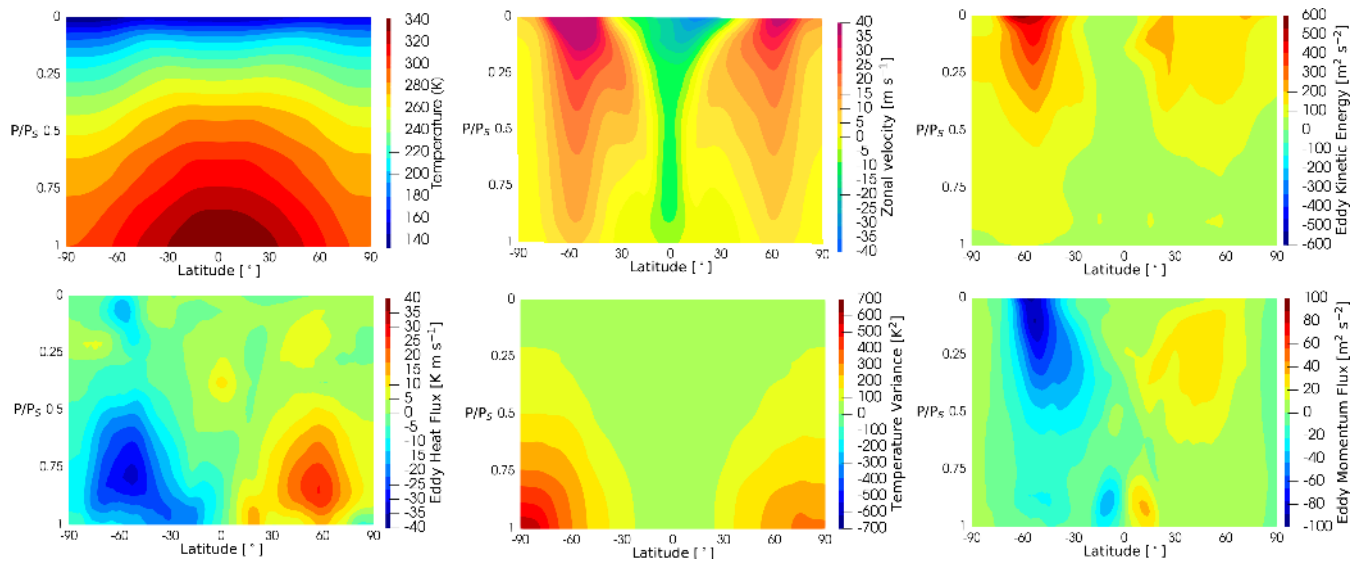
(a) Summer climatology: ADAPT 0.5.



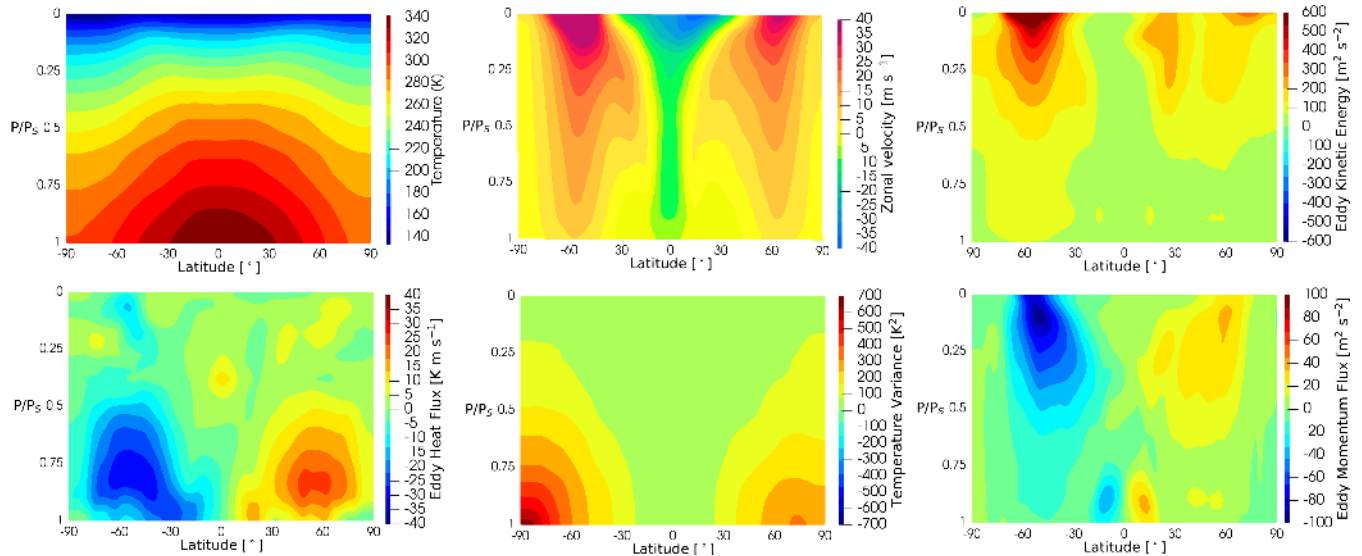
(b) Summer climatology: UNIF 0.5.

**Figure 4.** High resolution summer climatology of the adaptive and non-adaptive simulations. Statistics were averaged data saved every 5 days computed over the last 3 years of the 5 year run.

780 solstices, (see Figure 13), and at high altitudes where the kinetic energy density  $\frac{1}{2}\rho u^2$  is very low. The differences are small between  $-60^\circ\text{S}$  and  $60^\circ\text{N}$ . The exception is eddy heat flux, which has relatively large differences between  $-60^\circ\text{S}$  and  $30^\circ\text{S}$  in the summer. The relative  $l_2$  norm differences between ADAPT 0.5 and UNIF 0.5 are summarized in Table 4. The differences are in the range of 4–17% (except for temperature, which is much smaller, 0.5%). These quantitative errors are larger than the



(a) Fall climatology: ADAPT 0.5.

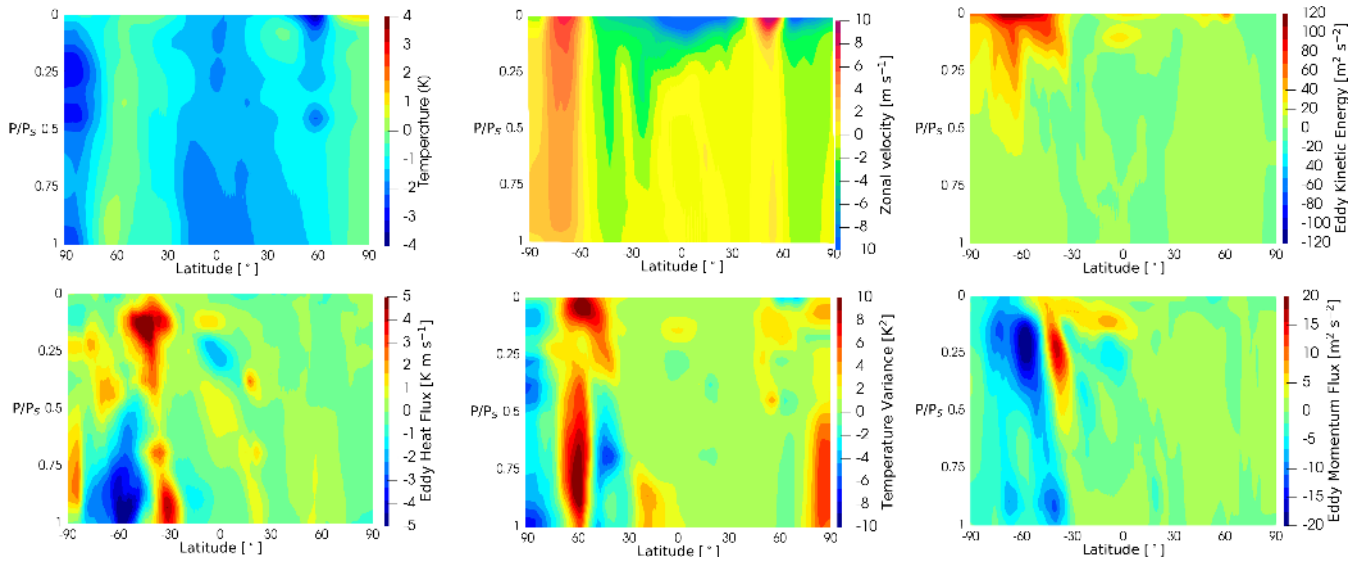


(b) Fall climatology: UNIF 0.5.

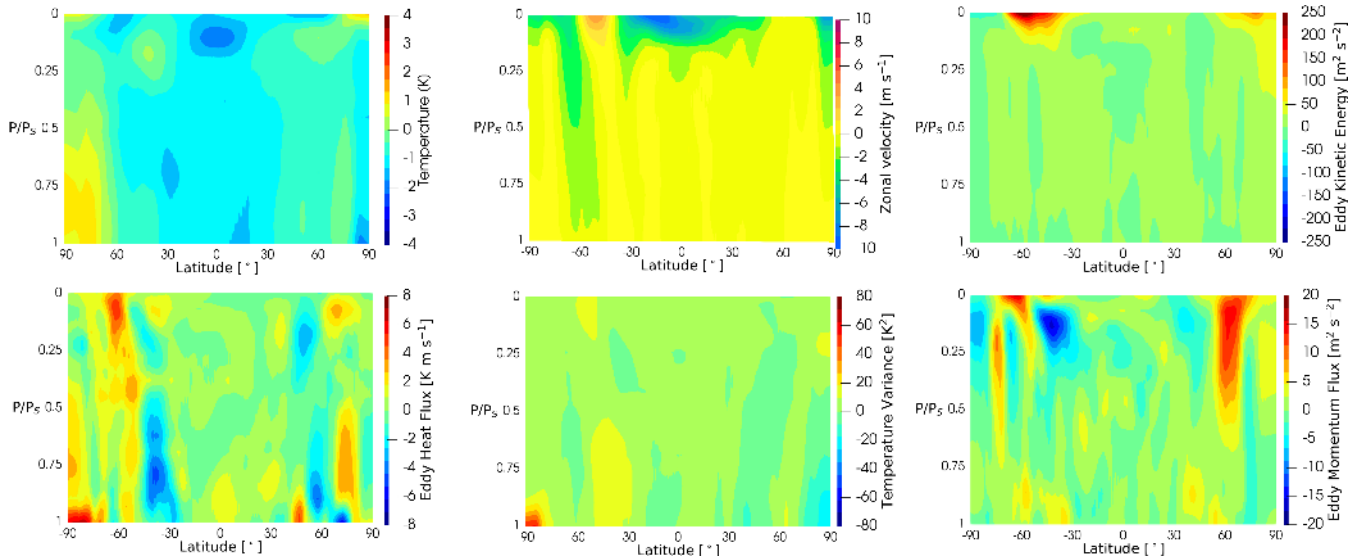
**Figure 5.** High resolution fall climatology of the adaptive and non-adaptive simulations. Statistics were averaged data saved every 5 days computed over the last 3 years of the 5 year run.

785 2.5% relative tolerance on the prognostic variables, which is perhaps unsurprising given the turbulent and unsteady nature of the climate dynamics.

In addition to the  $l_2$  errors between UNIF 0.5 and ADAPT 0.5, it is helpful to directly compare the meridional profile of vertically integrated second order statistics. Figure 7 shows vertically integrated eddy momentum flux for summer, fall and the



(a) Summer climatology: difference UNIF 0.5 - ADAPT 0.5.



(b) Fall climatology: difference UNIF 0.5 - ADAPT 0.5.

**Figure 6.** Difference between high resolution simulations UNIF 0.5 - ADAPT 0.5 for the summer and fall zonal climatology statistics. Note difference in scales compared to the climatology shown in Figures 4 and 5. The largest differences are at high altitudes and latitudes.

entire year for UNIF 2.0, UNIF 0.5 and ADAPT 0.5. These results confirm that that ADAPT 0.5 is much closer to UNIF 0.5 than the low resolution UNIF 2.0 is.

Field	Relative $l_2$ difference (summer)	Relative $l_2$ difference (fall)	Relative $l_2$ difference (full year)
Temperature	0.49%	0.12%	0.54%
Zonal velocity	15%	12%	13%
Eddy heat flux	8.7%	13%	18%
Eddy kinetic energy	13%	16%	10%
Eddy momentum flux	17%	16%	9.8%
Temperature variance	11%	4.1%	3.7%

**Table 4.** Relative  $l_2$  zonal climatology differences between the UNIF 0.5 and ADAPT 0.5 runs. The corresponding figures for summer and fall are shown in Figure 6.

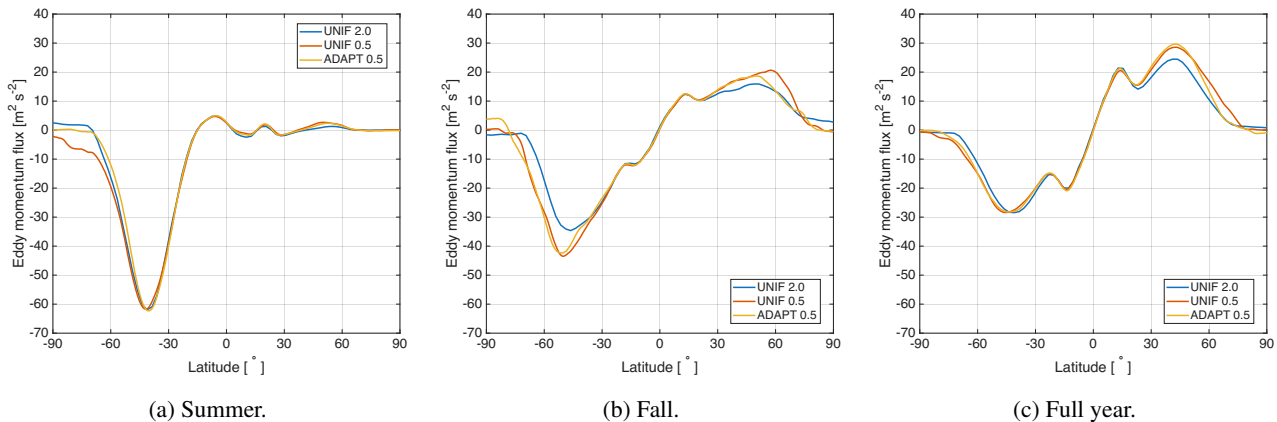


**Figure 7.** Vertically integrated eddy momentum flux for the UNIF 2.0, UNIF 0.5 and ADAPT 0.5 runs for summer, fall and full year.

### 790 4.3.2 Instantaneous temperature and vorticity dynamics

Climatology statistics do not directly provide any information about the dynamics, or “weather”, of the coupled dynamics–physics climate model. It is revealing to explore the instantaneous temperature and vorticity fields that determine the climate. In particular, we are interested in how the (turbulent) vorticity field changes with height and resolution and how well the adaptive method reproduces its small scale intermittent structure.

795 Figure 8 shows the instantaneous vorticity and temperature on 24 June of year 4 for layers 1, 9 and 27 (pressure levels 993 hPa, 713 hPa, 0.011 hPa respectively) for UNIF 0.5. The turbulence during the summer solstice is qualitatively different in the two hemispheres, with a narrow band of band of small scale turbulence centred around 30° N and large scale less intense turbulence extending over the entire southern hemisphere. This figure shows how the flow structure changes with height, with intense filamentary vorticity in the lower part of the atmosphere and smoother jet-like structures in the upper atmosphere. The  
800 temperature fields illustrate how the temperature is advected and mixed by the vorticity (like a passive scalar), with strong meridional temperature gradients.

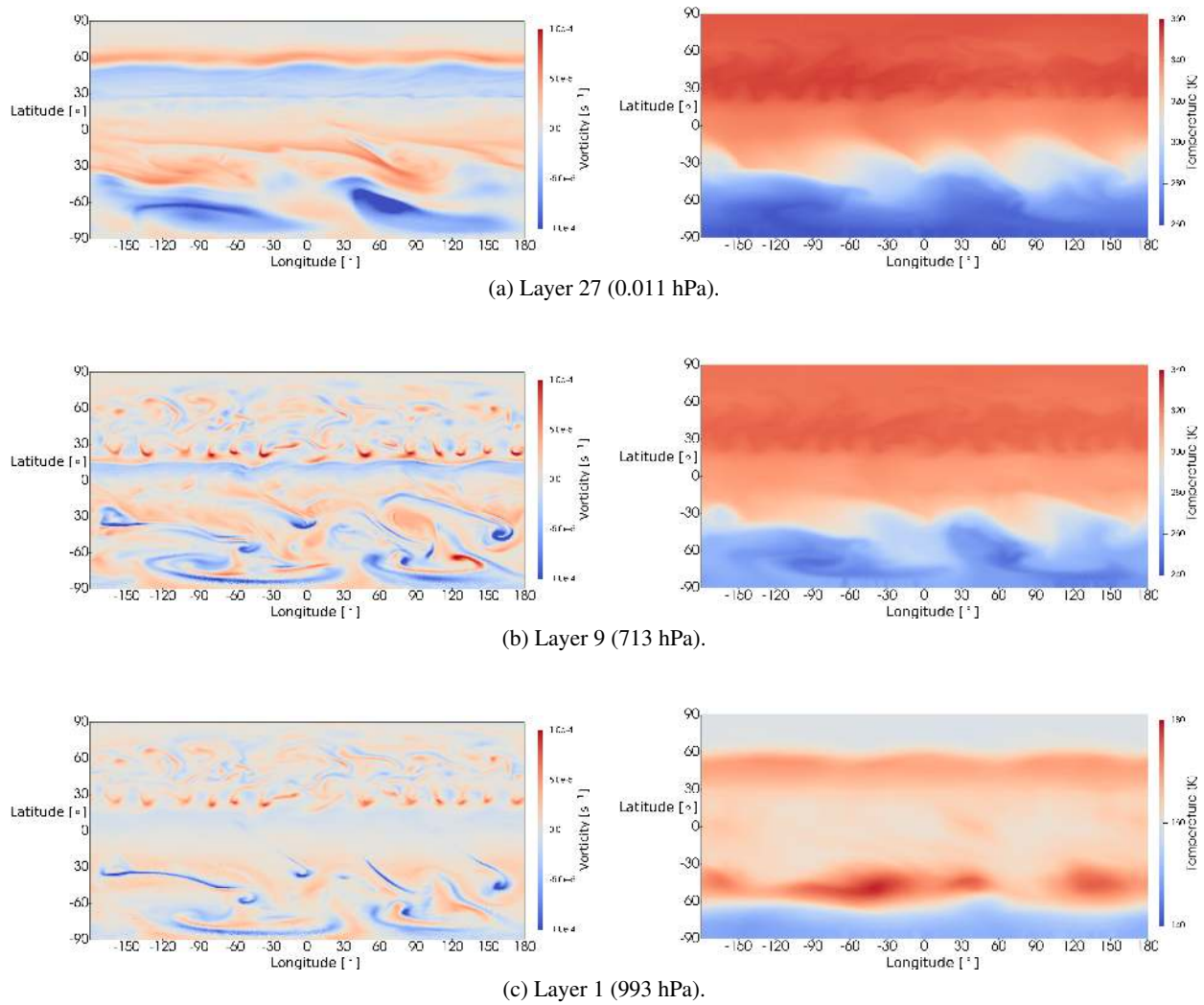
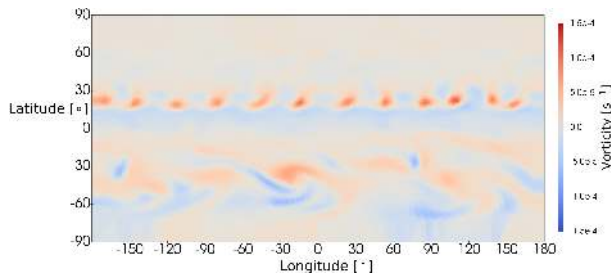
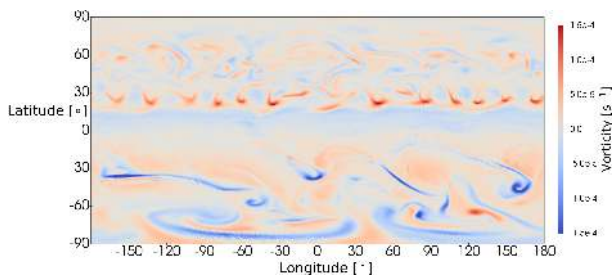


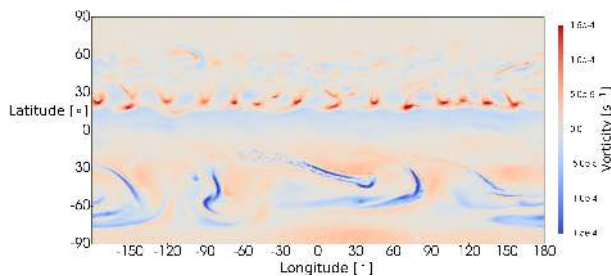
**Figure 8.** Vorticity and temperature near the summer solstice for UNIF 0.5 on 24 June of year 4 for three representative layers.



(a) UNIF 2.0 vorticity.



(b) UNIF 0.5 vorticity.



(c) ADAPT 0.5 vorticity.

**Figure 9.** Comparison of vorticity on 24 June of year 4 for layer 7 ( $P = 860$  hPa). The adaptive simulation ADAPT 0.5 captures the qualitative small scale structure of the non-adaptive UNIF 0.5 vorticity field. Note that since the dynamics are chaotic and non-stationary the locations of vorticity structures are not the same.

To evaluate how well the adaptive simulation captures the weather dynamics, Figure 9 at layer 7 (860 hPa) on 24 June of year 4, when the the weather is very different in the northern and southern hemispheres. ADAPT 0.5 is qualitatively similar to UNIF 0.5, capturing the qualitative features of the fine scale vorticity field. Note that we have set the relative tolerance to 2.5%, and the tolerance could be decreased (or increased) to balance computational cost and fidelity of the weather as desired. It is also important to note that because the flow is turbulent we cannot expect the details of the flow to match (e.g., shape and position of particular vortex filaments, number of eddies etc.). The adaptive grid shown in Figure 13 (bottom) shows that this difference in turbulence activity between the northern and southern hemispheres is reflected in the adaptive dynamical grid which has essentially no refinement north of about  $50^\circ$ . Comparing the instantaneous vorticity and temperature fields with the climatology statistics shown in Figures 4 gives a better understanding of how the instantaneous dynamics determines the climate.

Finally, Figure 10 shows isosurfaces of vorticity for the adaptive simulation on March 22 of year 5. The vorticity is primarily columnar, although there is some evidence of the intense atmospheric boundary layer structure visible in the eddy kinetic energy, eddy heat flux and eddy momentum flux shown in Figures 4,5. The primarily vertical vortices suggests that adapting only horizontally is efficient for these climate dynamics.

The preceding statistical and instantaneous results confirm that the dynamically adaptive GCM is stable and able to capture the emergence of small scale turbulence and the transitions between different seasonal dynamics. Furthermore, the

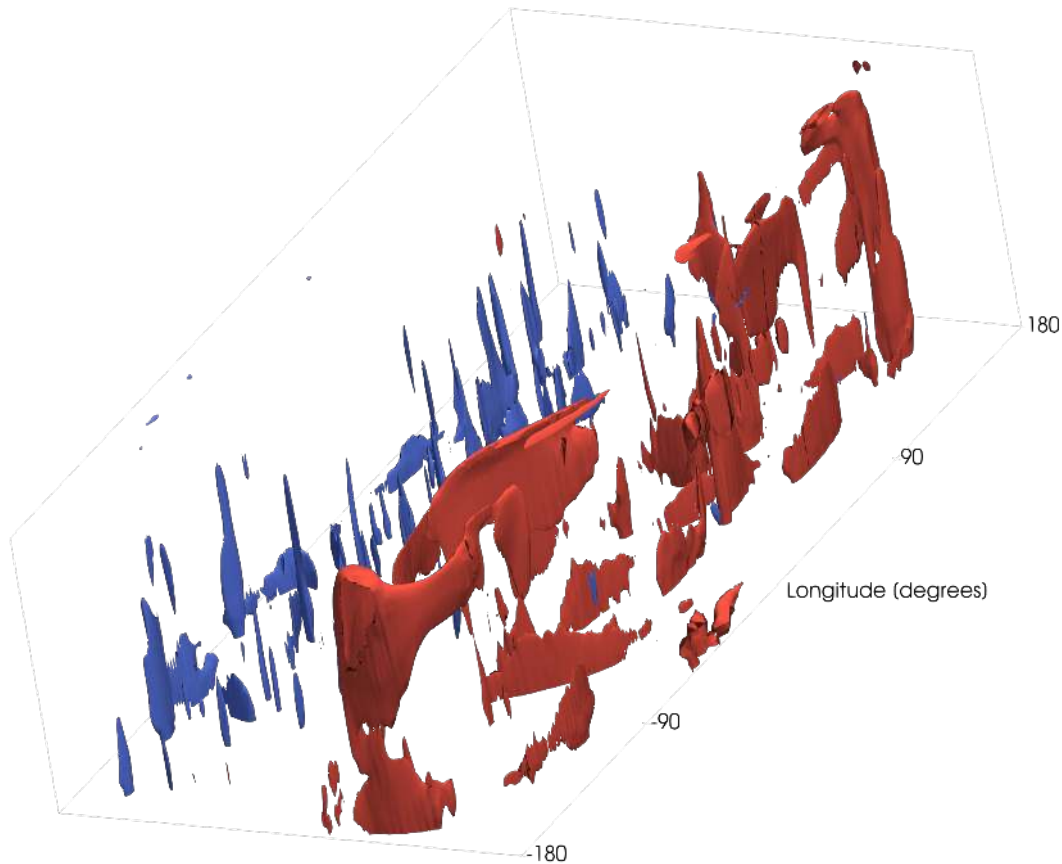


**Figure 10.** Isosurfaces of vorticity on March 22 of year 5 ( $\omega = \pm 10^{-4} \text{ s}^{-1}$ ) showing vertical structure of vorticity.

similarity of the high resolution adaptive climatology to the low resolution non-adaptive climatology suggests that adapting only on the prognostic variables is sufficient, at least for dry physics. The implicit effect of the physics on the dynamics is sufficient to resolve time- and scale-dependent dry physics phenomena.

We now show that the adaptive wavelet method reproduces the energy spectrum of the uniform high resolution simulation at all active length scales.

### 4.3.3 Energy spectra

A key feature of any GCM is the energy budget, and in order to properly represent turbulent atmosphere dynamics we need to ensure that the energy spectrum of the adaptive simulation is similar to that of the finest non-adaptive simulation is important over all length scales. Because the wavelet multiscale approach adapts in both position and length scale, one of its strengths is its ability to capture the full turbulent energy spectrum with a much smaller number of computational elements than an equivalent spectral method (Goldstein et al., 2005). We now verify that the adaptive simulation accurately captures the complete turbulent

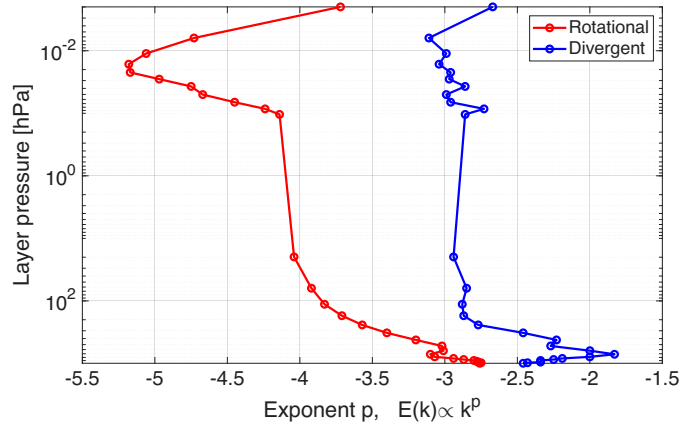


**Figure 11.** Energy spectra data averaged over year 5 for the non-adaptive  $0.5^\circ$  resolution case: spectral slope  $p$  for each layer obtained from linear fits for scales between 600 km and 2000 km. Note that the divergent spectra are much shallower than the rotational spectra and the flow is most turbulent (shallowest slope) at about 700 hPa.

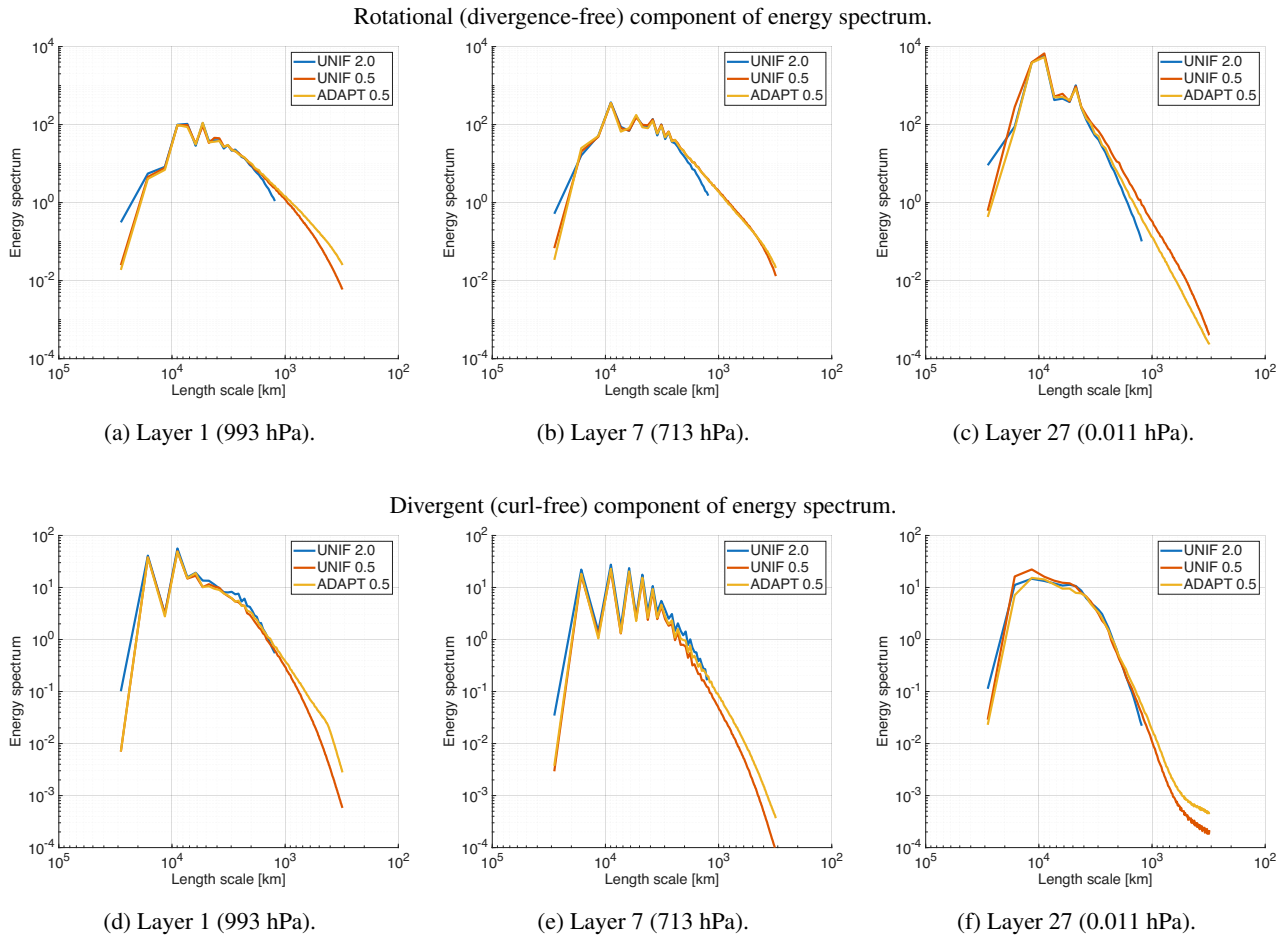
energy spectrum of the non-adaptive simulation. Since the flow is compressible, the rotational and divergent parts of the flow  
830 are both relevant. Recall that turbulence is characterized by a power law energy spectrum, where the power law  $p$ ,  $E(k) \propto k^p$  varies depending on the type of turbulence.

Figure 11 shows the power laws for each vertical layer for the  $0.5^\circ$  non-adaptive simulation. The slope  $p$  is found from linear fits on a log – log of energy spectrum for length scales between 600 km and 2000 km. The energy spectra were averaged over five years. The power laws for the  $0.5^\circ$  resolution simulations are between  $-1.8$  and  $-3$  for the divergent mode and be-  
835 tween  $-2.8$  and  $-5.2$ . For comparison, incompressible homogeneous isotropic three-dimensional turbulence has a power law of  $-5/3$ , while two-dimensional compressible turbulence has various spectra between  $-2$  and  $-4$ . Overall, the divergent component has a shallower slope, meaning that it is more turbulent. Furthermore, the flow is the most turbulent in the atmospheric boundary layer for  $P(z) > 600$  hPa.

Figure 12 compares the rotational and divergent components of the energy spectra of the non-adaptive (left) and adaptive  
840 (right) simulation. Results are shown for layers 1 (993 hPa), 9 (713 hPa) and 27 (0.0111 hPa). Figure 8 shows an example of the instantaneous vorticity and temperature structure for these layers. The energy spectra for the adaptive simulation are very similar to the non-adaptive spectra, but slightly smoother. Most importantly ADAPT 0.5 captures the full range of active length scales and the correct turbulent slopes but with about 3 times fewer computational modes (see §4.4 below).

#### 4.4 Computational performance of dynamic grid adaptivity

845 We begin by summarizing the quantitative and qualitative features of the dynamic grid adaptivity. The adaptive grid has an average compression ratio of 2.9, meaning that ADAPT 0.5 uses on average 2.9 times fewer active cells than UNIF 0.5. Over a simulation year the compression ratio varies depending on the season, with the highest compression at the solstices and the



**Figure 12.** Energy spectra averaged over year 5 for the three representative layers shown in Figure 8. We compare the low resolution uniform  $2^\circ$  simulation (UNIF 2.0), the high resolution uniform  $0.5^\circ$  simulation (UNIF 0.5) and the adaptive simulation (ADAPT 0.5). The adaptive simulation results have been interpolated to the finest resolution ( $0.5^\circ$ ) for the spectral analysis. The top row shows the rotational (divergence-free) component and the bottom row shows the divergent (curl-free) component of the energy spectrum. The adaptive results are consistent with the uniform high resolution results, apart from differences at the smallest scales. In particular, the adaptive simulation matches the spectral slope of the high resolution uniform simulation and resolves the full range of active scales.

lowest compression at the equinoxes, due to the changing weather patterns of the season. The maximum compression ratios of about 3.7 occur at the solstices and the minimum compression ratios of about 2.4 occur at the equinoxes. Figure 13 shows the adaptive grids with the lowest and highest compression ratios during the spring equinox on March 22 of simulation year 5 and during the summer solstice on June 25 of simulation year 4 respectively. At the summer solstice the northern (hotter) hemisphere is less active than the southern (cooler) hemisphere. Overall, the atmosphere is much less turbulent at the solstices than at the equinoxes. The annual pattern of grid compression is clear in Figure 14. These results confirm the ability of the

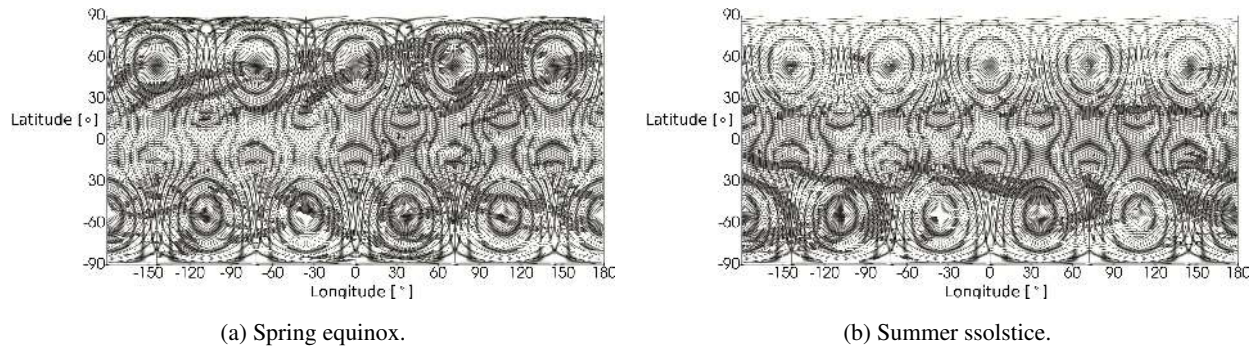


**Figure 13.** Adaptive dual triangular grids from ADAPT 0.5 simulation with tolerance 2.5%. (a) On 5 March 22 of year 5, during an equinox. (b) On June 25 of year 4, during a summer solstice. At the summer solstice the northern (hotter) hemisphere is less active than the southern (cooler) hemisphere, leading to a higher compression ratio.

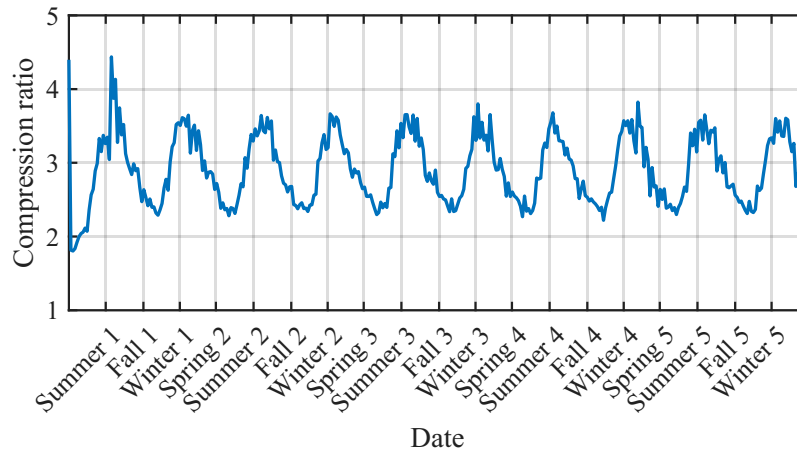
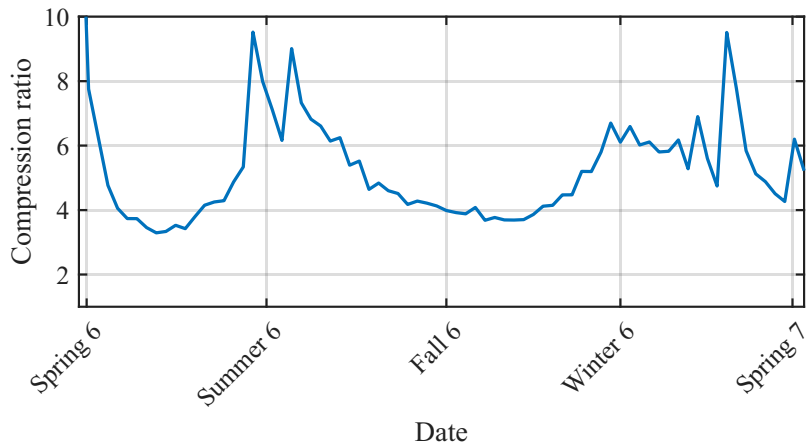


**Figure 14.** Compression ratio for the ADAPT 0.5 run with relative tolerance 2.5% showing seasonal variation over 5 years. The solstices and equinoxes are labelled. The highest compression ratios are at the solstices and the lowest compression ratios are at the equinoxes.

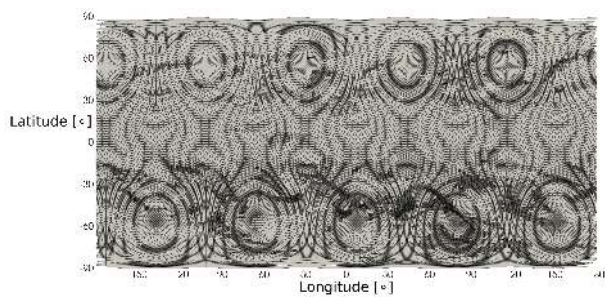
adaptive grid to refine and coarsen, both locally in space and following the seasons, as required to capture the dynamically important features of the flow.

855 Finally, we investigate whether a low resolution simulation can be stably restarted from a saved checkpoint at much higher dynamically adaptive resolution. This allows investigation of climate dynamics at higher resolutions for shorter periods of time and permits quickly spinning up the model at low resolutions. We restarted from a non-adaptive UNIF 2.0 checkpoint at 5 years (March 22), with maximum resolution increased by 8 times to  $0.25^\circ$ . This corresponds to a 64 times increase in horizontal resolution. We ran the simulation for an additional one year. This run is referred to as ADAPT 0.25.

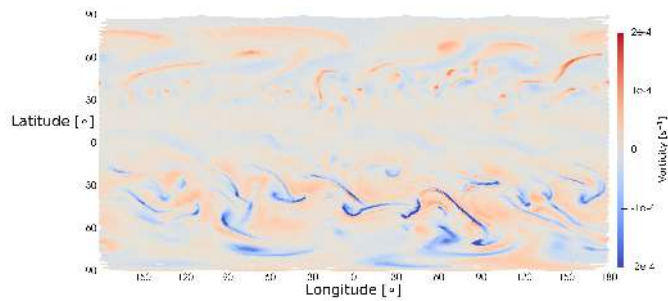
860 Figure 15 (top) shows the grid compression ratio as a function of time and Figure 15 (middle) shows the adapted horizontal grid 95 days after restarting. The relative tolerance is the same as for ADAPT 0.5,  $\varepsilon = 2.5\%$ . The restarted high resolution sim-



(a) Compression ratio for ADAPT 0.25.



(b) Adaptive grid for year 6 March 22.



(c) Layer 7 (860 hPa) vorticity field for year 6 March 22.

**Figure 15.** Results for ADAPT 0.25 simulation restarted after 5 years from UNIF 2.0 with relative tolerance  $\varepsilon = 2.5\%$ . The average compression ratio is 5.3.

865  
 ulation ran stably with an average grid compression ratio of 5.3. After start-up, the grid compression varied between 3.3 and 9.5, depending on the season. Adding one more resolution level achieves an average compression ratios almost twice as large as ADAPT 0.5, with maximum compression ratios 2.6 times higher. The corresponding vorticity field shown in Figure 15 (bottom) illustrates how the adaptive grid tracks the intense vorticity filaments. This result shows the potential of adaptivity to both achieve relatively high grid compression (and corresponding speed-up) and the ability to investigate higher horizontal resolutions for shorter periods.

## 5 Conclusions

870 This paper presents the results of coupling a simple dry physics sub-grid scale model to the WAVETRISK-ATMOSPHERE dynamical core. We have four main goals:

1. Fully document the approximations and numerical implementation of the simple dry physics model introduced by Hourdin (1992).
2. Couple the simple physics package to the WAVETRISK-ATMOSPHERE multiscale adaptive dynamical core. To do this, the simple physics code has been rewritten in FORTRAN 2008 and simplified.
3. Describe the 5-year climatology of the WAVETRISK–simple physics climate model, run non-adaptively at coarse resolution  $2^\circ$  with 30 vertical atmosphere layers and 10 soil layers. The results without and with seasons are compared to an equivalent Held and Suarez (1994) climate model.
4. Explore an adaptive WAVETRISK–simple physics climate model coupling and assess the need for scale aware parameterizations or grid adaptation criteria. The coarsest resolution is  $2^\circ$  and we allow two layers of refinement:  $1^\circ$  and  $0.5^\circ$ , for a maximum grid compression ratio of 16 times. The adaptive results are compared with an equivalent non-adaptive  $0.5^\circ$  resolution simulation.

The basic approximations of the physical model are: dry atmosphere (i.e., no moisture), hydrostatic balance, compressibility and a floating vertical coordinate. The physics model is coupled to the dynamics as an implicit split step in time. It includes sub-grid scale parameterizations for radiation, vertical turbulent diffusion of velocity and potential temperature, a planetary boundary layer, surface fluxes, dry convection, diurnal cycle, seasons and, significantly, a soil column. The lack of moisture reduces model realism, but maintains simplicity and simplifies the interpretation of results. Model parameters, such as gravity and astronomical parameters, are set to Earth values.

Compared to the Held & Suarez and the International Standard Atmosphere, the temperature profile for the simple physics–WAVETRISK climate model decreases is significantly warmer near the surface of the atmosphere and decreases monotonically with height. These differences are likely due to two limitations of the simple dry physics package, specifically the lack of moisture and the simplicity of the radiation parameterization (e.g., no ultraviolet absorption band in the stratosphere). We presented zonal statistics of temperature, zonal velocity, eddy kinetic energy, eddy heat flux, temperature variance and eddy momentum flux. Without seasons, these statistics are qualitatively similar to those of the Held & Suarez model, although the location of zonal jets is shifted and the eddy kinetic energy is about half as strong. This suggests the additional slow time scales introduced by the soil column do not significantly affect the climatology. Unsurprisingly, adding seasons dramatically modifies all statistical quantities.

The adaptive simple physics–WAVETRISK climate model with horizontal resolutions  $2^\circ$ ,  $1^\circ$ ,  $0.5^\circ$  is stable and accurate. With relative tolerance 2.5% produces grid compression ratios of between about 1.8 times (at the equinoxes) and 3.0 times (at the solstices). This demonstrates the efficiency advantages of horizontal grid adaptivity, as it is able to track the active and inactive parts of the globe throughout the year. The zonal statistics are very similar to those of the  $2^\circ$  non-adaptive simulation and also agree well with the non-adaptive  $0.5^\circ$  results.

In addition to comparing the 5-year statistics, we also compared longitude-latitude projections of vorticity for the adaptive and non-adaptivity simulations on 25 June of year 4 when there is a strong north-south asymmetry in the turbulence. The

905 weather is characterized by a narrow band of small scale turbulence centered around 30° N and a large scale less intense turbulence extending over the entire southern hemisphere. The adaptive simulation successfully captures the large and small scale vortical structures in each hemisphere. Finally, we presented isosurfaces of vorticity for March 22 of year 5. The vorticity is primarily columnar, but also includes intense atmospheric boundary layer structures, which are also visible in the statistics.

To complement the physical space comparisons, we compared energy spectra for the rotational and divergent components  
910 for adaptive and non-adaptive simulations. These results confirm that the adaptive simulation accurately captures the full range of active turbulent scales, although there is some smoothing due to interpolation of the adaptive grid onto the full grid (needed to compute the spherical harmonics transform). Vertical profiles of the energy spectrum power law show strong dependence on depth, with the most turbulent region in the boundary layer,  $P(z) > 600$  hPa.

Overall, we conclude that the simple dry physics model can be stably coupled to an adaptive dynamical core. Scale-aware  
915 parameterizations are not necessary, at least for dry physics.

The climatology presented here could provide the basis for new dynamical core test cases since the simple dry physics can be easily coupled to different dynamical cores. The simple physics includes relatively sophisticated radiation, turbulence, convection and diurnal/seasonal forcing and thus fills a gap between the Held & Suarez model and realistic moist physics models. Future work could explore an intercomparison of a set of dynamical cores coupled to the same simple dry physics  
920 package.

Although scale-aware physics parameterization is not necessary for this dry physics model, it is quite likely to be necessary for moist physics. In future work, we will investigate coupling the adaptive WAVETRISK model to a basic moist physics, such as Kessler (1969). This model has already been coupled to the Held & Suarez model Ullrich et al. (2016).

We hope that the results presented here will stimulate interest in Hourdin (1992)'s interesting dry physics model and has  
925 demonstrated the potential of adaptive dynamical cores to improve the efficiency and accuracy of climate modeling. Our results may also help climate modelers simplify the tuning required when grid resolution is increased by focusing their attention on sub-models not included in the simple dry physics.

*Code and data availability.* The WAVETRISK code, including the simple dry physics and Held–Suarez physics, are available at [https://github.com/kevlahan/wavetrisk\\_hydrostatic](https://github.com/kevlahan/wavetrisk_hydrostatic). The test case `/test/climate` is used to run the simulations. The data presented in this paper are  
930 available at this globus link: Globus .

## Appendix A: Software Engineering Design Decisions and Challenges

To couple the simple dry physics package to the dynamical core WAVETRISK certain design decisions were made in order to facilitate the physics-dynamics coupling and overcome challenges encountered due to dynamic adaptivity. This appendix section will summarize the general steps needed to couple the simple dry physics package to a dynamical core and the decisions  
935 made to couple the package to WAVETRISK.

In order to utilize the physics package as a test case and couple it with a dynamical core an interface is used. This interface is the connector and facilitator of the entire model and will vary among climate models due to different dynamical core architectures and their methods of incorporating test cases. In terms of coupling the physics to WAVETRISK, we made the design decision to create an interface formatted as one of WAVETRISK's test cases. The interface calls all physics initialization routines  
940 through a wrapper function which includes setting up the plugins of the physics and reading all constants and constraints set by the dynamics. As the facilitator, the interface couples the dynamics and physics by calling their associated time step routines, usually in a split step. When calling the physics time step a few aspects need to be taken into account, the precision of the both the dynamics and physics, the format of the main prognostic variables stored and the data structures of the prognostic variables, which is highly dependent on the grid.

945 The physics package is written in single precision, while WAVETRISK is written in double precision. To avoid converting to and from both data types, before and after the physics step, we decided to compile the physics package with the Fortran flag, `-freal-4-real-8`. This flag converts all real numbers (single precision) in the physics package to real (8) values (double precision), allowing for compatibility with WAVETRISK.

The key input variables required for a physics package time step includes temperature, zonal velocity and meridional ve-  
950 locity at each vertical layer, along with the pressure and geopotential of the vertical columns. Calculating the pressure and geopotential requires the simple integration from the surface upwards for each column and the utilization of the hydrostatic approximation. In comparison, the temperature and velocities require a more in-depth conversion. WAVETRISK saves the mass weighted potential temperature as its prognostic variable. Therefore, when calling the physics, the interface converts the value, at each vertical layer of a column, to potential temperature and then to the required temperature input, in Kelvin, of the physics.  
955 Upon return from the physics call, the interface converts the temperature tendencies back to mass weighted potential temperature using the reverse process. Regarding the zonal and meridional velocities, wavetrisk does not store the velocities at the center of the node, instead it stores three velocity edge values. To retrieve the zonal and meridional velocities at the node, interpolation using the three edge values and neighbouring columns' edge values is required. The inverse procedure is also applied when the physics returns the zonal and meridional tendencies for each column.

960 In general, the data structures storing the prognostic variables of both the dynamics and physics are different. WAVETRISK utilizes a hybrid data structure which is optimal for the grid chosen and for adaptivity and load balancing associated with the use of parallelism (see (Aechtner et al., 2014) for more on the WAVETRISK grid architecture and data structure). Conversely, the physics package utilizes a regular data structure to store the values for each column. The regular data structure is a 2D array, with each row representing a different vertical column and each column of the array represents a vertical layer. Upon  
965 initialization of the physics package, the number of vertical columns to be sent at each time step is fixed. At each physics step, the package takes in the fixed number of vertical columns, the time step, the simulation day, the fraction of the day and the columns' prognostic variable values, pressure and geopotential at each vertical layer. A major overhead of the simulation, even in the case of parallelism, is the retrieval and conversion of all vertical columns from the hybrid data structure to the required regular structure for the input of the prognostic variables, as well as the conversion of the output tendencies from the regular to  
970 hybrid data structure.

The use of a 2D data structure constrains the package as it expects the user to call the physics for all vertical columns at once. However, another major obstacle this structure produces is in the case of parallelism and adaptivity. WAVETRISK utilizes `mpi` and domain decomposition of the columns of the sphere. When adaptivity is used, a major concern is ensuring correct load balancing on each CPU. Therefore, WAVETRISK allows for the re-balancing of the domains on each CPU, to ensure approximately equal computational loads. The complication arising with the ability of rebalancing is that the physics package saves the soil and surface temperatures internally for each column. To reduce the overhead and overcome the rebalancing obstacle, we have modified the physics step to call the physics for vertical columns individually and the step is completed when the last column's tendency returns from the call. However, to allow for single column transmission, the physics package and WAVETRISK required some fine tuning and additions.

The major addition to the physics package is the creation of the single column module. It allows the model to call the physics package for each column individually by providing the soil and surface temperatures to the dynamics. This module contains a wrapper subroutine that the interface calls, including all required inputs for the original physics call plus the added soil and surface temperatures. Once the wrapper subroutine is called, it updates the soil and surface temperatures for the column and calls the original physics routine. The subroutine outputs the original tendencies and the new updated soil and surface temperatures for the interface to save. The module also contains a subroutine that allows for the change in latitude and longitude required when sending a different column at each physics call. A major change to the physics package is the input of the number of desired soil layers when initializing the parameters of the grid in the package. Originally this was fixed to 10, but a variable number of layers is desired to test the importance of the soil model.

The only major change to WAVETRISK was in the grid initialization. To send single columns to the physics with the possibility of rebalancing, WAVETRISK must save the soil temperatures and surface temperature of each column. The vertical layers were therefore extended, below the surface, employing negative and zero indexes for each vertical column to represent the soil layers ( $k < 0$ ) and surface ( $k = 0$ ) temperature respectively. The interface facilitates this by setting the number of soil layers, before all grids are initialized. The only drawback of extending the grid is that all prognostic variables' data structures need to be extended, even though only the mass-weighted potential temperature negative indexes are used to save the soil and surface values. Therefore, there is additional unnecessary memory overhead. In future, it is recommended that only the required variable's data structure be extended, but this will require a more extensive update, not only to the architecture of the grid, but also to the architecture of the calls for the dynamics step.

Another WAVETRISK design decision was the format and storage of the extra temperature values. It was decided that the soil and surface temperatures would be stored in the mass-weighted potential temperature's data structure in the negative and 0 indexes respectively. More importantly, the temperatures would not be converted to mass-weighted potential temperature, but would be retained as temperature (units of Kelvin). This decision was made to avoid the extra overhead that comes with the conversion, as the values are not used by the dynamics.

Finally, while the main decision to send individual grid columns to the physics required extra temperature values to be stored by the dynamics, no other physics variables need to be stored. In many models, as in the WAVETRISK-OCEAN model configuration, a new dynamics variable `tke` is required to keep track of the turbulent kinetic and the `tke` evolves over time with

the physics' k-epsilon model. However, since the simple physics model's vertical diffusion is a first order closure model, no further variables need to be stored and the interpolation of any internal physics variables onto the adaptive grid is not required.

### **A1 The workflow of the interface and physics call**

1010 To illustrate the sequence of steps taken by the interface Fig. A1 displays the workflow of the interface written to couple WAVETRISK to the physics package. Furthermore, to illustrate the physics-dynamics coupling challenges mentioned above, Fig. A2 displays a flowchart of the algorithm used by the interface and required for the a single physics (split) step. The steps in black are the extra steps required to change prognostic variables to the required form, for example mass-weighted potential temperature to temperature or vice versa. The yellow step represents the call to the wrapper subroutine in the single column module added to physics package to allow the architecture of sending individual columns.

1015 *Author contributions.* F Hourdin developed the original simple physics model in his PhD thesis. GCJ, NKRRK prepared the paper with contributions from TD. NKRRK developed the model code with contributions from GCJ and TD for the dry physics module. GCJ and NKRRK performed the model simulations using WAVETRISK-ATMOSPHERE.

*Competing interests.* The contact author has declared that none of the authors has any competing interests.

1020 *Acknowledgements.* NKRRK and GCJ were supported by the Natural Sciences and Engineering Research Council of Canada (NSERC) under grant no. RGPIN-2024-05282.

## References

- Aechtner, M., Kevlahan, N. K.-R., and Dubos, T.: A conservative adaptive wavelet method for the shallow-water equations on the sphere, *Quarterly Journal of the Royal Meteorological Society*, 141, 1712–1726, <https://doi.org/10.1002/qj.2473>, 2014.
- Arya, S. P.: Chapter 4 Soil Temperatures and Heat Transfer, in: *Introduction to Micrometeorology*, vol. 42 of *International Geophysics*, pp. 37–48, Academic Press, [https://doi.org/https://doi.org/10.1016/S0074-6142\(08\)60419-2](https://doi.org/https://doi.org/10.1016/S0074-6142(08)60419-2), 1988.
- Collins, S. N., James, R. S., Ray, P., Chen, K., Lassman, A., and Brownlee, J.: Grids in Numerical Weather and Climate Models, in: *Climate Change and Regional/Local Responses*, edited by Zhang, Y. and Ray, P., chap. 4, IntechOpen, <https://doi.org/10.5772/55922>, 2013.
- Ferguson, J. O., Jablonowski, C., Johansen, H., McCorquodale, P., Colella, P., and Ullrich, P. A.: Analyzing the Adaptive Mesh Refinement (AMR) Characteristics of a High-Order 2D Cubed-Sphere Shallow-Water Model, *Monthly Weather Review*, 144, 4641 – 4666, <https://doi.org/https://doi.org/10.1175/MWR-D-16-0197.1>, 2016.
- Frassoni, A., Castilho, D., Rixen, M., Ramirez, E., de Mattos, J. G. Z., Kubota, P., Calheiros, A. J. P., Reed, K. A., da Silva Dias, M. A. F., da Silva Dias, P. L., de Campos Velho, H. F., de Roode, S. R., Doblas-Reyes, F., Eiras, D., Ek, M., Figueroa, S. N., Forbes, R., Freitas, S. R., Grell, G. A., Herdies, D. L., Lauritzen, P. H., Machado, L. A. T., Manzi, A. O., Martins, G., Oliveira, G. S., Rosário, N. E., Sales, D. C., Wedi, N., and Yamada, B.: Building the Next Generation of Climate Modelers: Scale-Aware Physics Parameterization and the “Grey Zone” Challenge, *Bulletin of the American Meteorological Society*, 99, ES185 – ES189, <https://doi.org/https://doi.org/10.1175/BAMS-D-18-0145.1>, 2018.
- Goldstein, D. E., Vasilyev, O. V., and Kevlahan, N. K.-R.: CVS and SCALES Simulation of 3-D Isotropic Turbulence, *Journal of Turbulence*, 6, 1–20, <https://doi.org/10.1080/14685240500460790>, 2005.
- Held, I. and Suarez, M.: A Proposal for the Intercomparison of the Dynamical Cores of Atmospheric General Circulation Models, *Bulletin of the American Meteorological Society*, 76, 1825–1830, 1994.
- Honnert, R.: Representation of the grey zone of turbulence in the atmospheric boundary layer, *Advances in Science and Research*, 13, 63–67, <https://doi.org/10.5194/asr-13-63-2016>, 2016.
- Hourdin, F.: Étude et simulation numérique de la circulation générale des atmosphères planétaires, Phd thesis, Université de Paris 7, 1992.
- Jablonowski, C. and Williamson, D. L.: A baroclinic instability test case for atmospheric model dynamical cores, *Quarterly Journal of the Royal Meteorological Society*, 132, 2943–2975, <https://doi.org/https://doi.org/10.1256/qj.06.12>, 2006.
- Jablonowski, C., Herzog, M., Penner, J. E., Oehmke, R. C., Stout, Q. F., and van Leer, B.: Adaptive Grids for Weather and Climate Models, in: *Seminar on Recent Developments in Numerical Methods for Atmospheric and Ocean Modelling*, pp. 233–250, ECMWF, Shinfield Park, Reading, UK, 2004.
- Kent, J., Ullrich, P. A., and Jablonowski, C.: Dynamical core model intercomparison project: Tracer transport test cases, *Quarterly Journal of the Royal Meteorological Society*, 140, 1279–1293, <https://doi.org/https://doi.org/10.1002/qj.2208>, 2014.
- Kessler, E.: On the Distribution and Continuity of Water Substance in Atmospheric Circulations, no. 10 in *Meteorological Monographs*, American Meteorological Society, Boston, MA, [https://doi.org/10.1007/978-1-935704-36-2\\_1](https://doi.org/10.1007/978-1-935704-36-2_1), 1969.
- Kevlahan, N. K. R. and Dubos, T.: WAVETRISK-1.0: An adaptive wavelet hydrostatic dynamical core, *Geoscientific Model Development*, 12, 4901–4921, <https://doi.org/10.5194/gmd-12-4901-2019>, 2019a.
- Kevlahan, N. K.-R. and Dubos, T.: WAVETRISK-1.0: an adaptive wavelet hydrostatic dynamical core, *Geoscientific Model Development*, 12, 4901–4921, <https://doi.org/10.5194/gmd-12-4901-2019>, 2019b.

- Kevlahan, N. K.-R. and Lemarié, F.: WAVETRISK-2.1: An adaptive dynamical core for ocean modelling, *Geoscientific Model Development*, 15, 6521–6539, <https://doi.org/10.5194/gmd-15-6521-2022>, 2022.
- 1060 Lauritzen, P. H., Kevlahan, N. K.-R., Toniazzo, T., Eldred, C., Dubos, T., Gassmann, A., et al.: Reconciling and Improving Formulations for Thermodynamics and Conservation Principles in Earth System Models (ESMs), *Journal of Advances in Modeling Earth Systems*, 14, e2022MS003117, <https://doi.org/10.1029/2022MS003117>, 2022.
- Louis, J.: A parametric model of vertical eddy fluxes in the atmosphere, *Boundary-Layer Meteorology*, 17, 187–202, <https://doi.org/https://doi.org/10.1007/BF00117978>, 1979.
- 1065 Park, H., Kim, G., Cha, D.-H., Chang, E.-C., Kim, J., Park, S.-H., and Lee, D.-K.: Effect of a Scale-Aware Convective Parameterization Scheme on the Simulation of Convective Cells-Related Heavy Rainfall in South Korea, *Journal of Advances in Modeling Earth Systems*, 14, e2021MS002696, <https://doi.org/https://doi.org/10.1029/2021MS002696>, e2021MS002696 2021MS002696, 2022.
- Phillips, N. A.: The general circulation of the atmosphere: A numerical experiment, *Quarterly Journal of the Royal Meteorological Society*, 82, 123–164, <https://doi.org/10.1002/qj.49708235202>, 1956.
- Pierrehumbert, R. T.: *Principles of Planetary Climate*, Cambridge University Press, <https://doi.org/10.1017/CBO9780511780783>, 2010.
- 1070 Ringler, T. D., Thuburn, J., Klemp, J. B., and Skamarock, W. C.: A unified approach to energy conservation and potential vorticity dynamics for arbitrarily-structured C-grids, *J. Comput. Phys.*, 229, 3065–3090, <https://doi.org/10.1016/j.jcp.2009.12.007>, 2010.
- Skamarock, W., Oliger, J., and Street, R. L.: Adaptive grid refinement for numerical weather prediction, *Journal of Computational Physics*, 80, 27–60, [https://doi.org/https://doi.org/10.1016/0021-9991\(89\)90089-2](https://doi.org/https://doi.org/10.1016/0021-9991(89)90089-2), 1989.
- 1075 St-Cyr, A., Jablonowski, C., Dennis, J. M., Tufo, H. M., and Thomas, S. J.: A Comparison of Two Shallow-Water Models with Nonconforming Adaptive Grids, *Monthly Weather Review*, 136, 1898 – 1922, <https://doi.org/https://doi.org/10.1175/2007MWR2108.1>, 2008.
- Ullrich, P. A., Jablonowski, C., Kent, J., Lauritzen, P. H., Nair, R. D., Reed, K. A., Zarzycki, C. M., and ...: Dynamical Core Model Inter-comparison Project (DCMIP) Test Case Document, Technical report, University of Michigan, includes Fortran initialization routines for tracer-transport test cases, 2012.
- 1080 Ullrich, P. A., Jablonowski, C., and Holland, D. M.: A moist Held–Suarez test case for idealized model intercomparisons, *Journal of Advances in Modeling Earth Systems*, 8, 178–195, <https://doi.org/10.1002/2015MS000447>, 2016.

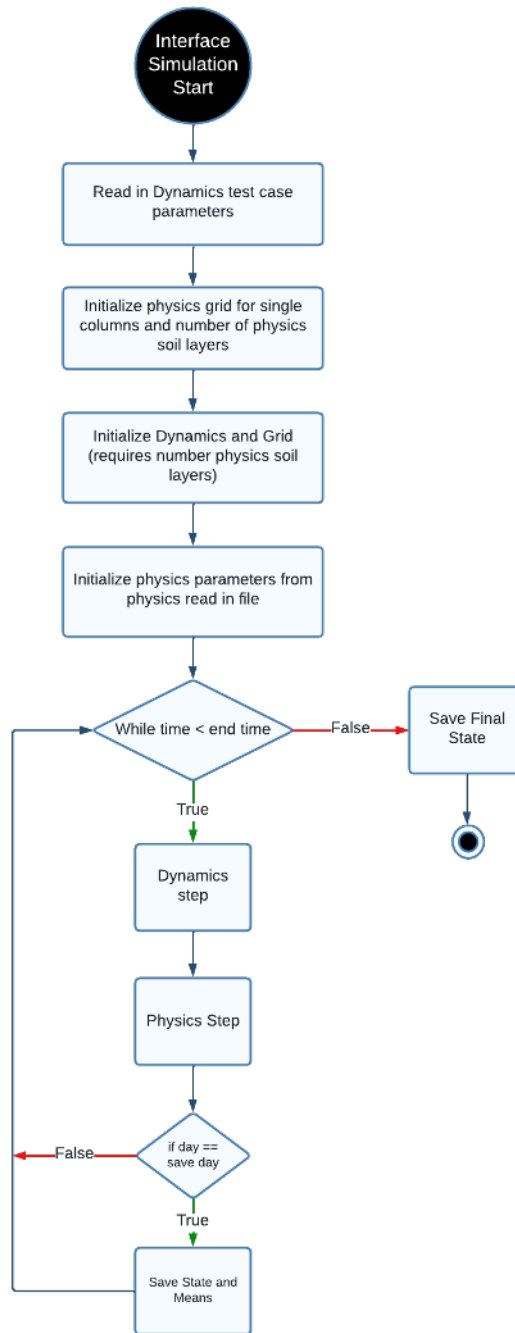


**Figure A1.** A flow chart of the interface (physics-dynamics) coupling the physics and dynamics. The workflow shows the the steps of the simulation until the end.

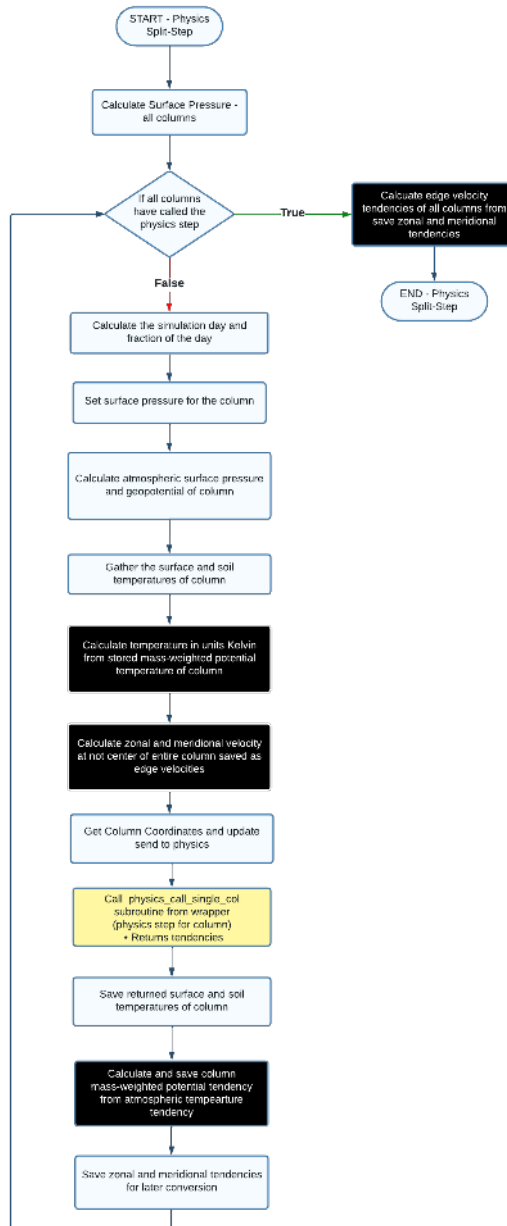


**Figure A2.** A flow chart of the physics step. Steps in black contain overhead concerning the conversion of the prognostic variables from one type to another (i.e. mass-weighted potential temperature to temperature ( $K$ )). The yellow process represents the physics call of the added single column module of the physics.